Article:
Colombera, L, Arévalo, OJ and Mountney, NP (2017) Fluvial-system response to climate change: The Palaeocene-Eocene Tremp Group, Pyrenees, Spain. Global and Planetary Change, 157. pp. 1-17. ISSN: 0921-8181

https://doi.org/10.1016/j.gloplacha.2017.08.011

Fluvial-system response to climate change: the Paleocene-Eocene Tremp Group, Pyrenees, Spain

Luca Colombera[1]*, Oscar J. Arévalo[1], Nigel P. Mountney[1]

1) Fluvial & Eolian Research Group, School of Earth and Environment, University of Leeds, UK.

**) E-mail: l.colombera@leeds.ac.uk*

Abstract

The Tremp Group of the Tremp-Graus Basin (Southern Pyrenees, Spain) is a succession of predominantly continental origin that records the Paleocene-Eocene Thermal Maximum (PETM), a transient episode of extreme global warming that occurred across the Paleocene-Eocene boundary. For this succession, the stratigraphic position of the PETM is accurately determined, and histories of tectonic and sea-level controls are well constrained. Building upon previous studies, this work assesses changes in sedimentary architecture through the PETM in the Tremp Group, based on quantitative sedimentological analyses documented over a km-scale strike-oriented transect in the Arén area, with the scope to better understand the response of this alluvial system to the hyperthermal event. The analysed features represent a partial record of the geomorphic organization and processes of the system at the time of deposition, and are therefore interpretable in terms of geomorphic change in alluvial landscapes caused by the PETM.

The record of the PETM, as previously recognized, begins at a time when erosional palaeotopographic relief was developed and deposition was confined in valleys. A shift between valley back-filling and widespread aggradation is observed at the onset of the PETM interval, which demonstrates uniquely the impact of the hyperthermal on both depositional loci and interfluves. Compared to underlying strata, the interval that embodies the onset and main phase of the PETM is characterized by: (i) higher proportion of channel deposits; (ii) channel complexes of greater average thickness and width; (iii) barforms and channel fills that are slightly thicker; (iv) increased thickness of sets of cross-stratified sandstones; (v) similar values of maximum extraclast size, by

architectural element. An evident change in the facies organization of channel deposits is also seen through the stratigraphy, though this appears to predate the PETM.
Increased channel-body density in the PETM interval can be explained in terms of increased channel mobility, which itself can be related to changes in the stream catchments (e.g., greater bedload delivery, increased water discharge or discharge variability), or to changes in the nature of the depositional basin that would permit the channels to be more mobile (e.g., increased bank erodibility due to variations in vegetation type and density). Interfluve planation is inferred to have occurred immediately prior to, or penecontemporaneously with, accumulation of PETM deposits, which is in accord with inferences of increased erodibility of the interfluves or increased stream erosive power. These observations offer insight into the potential geomorphic metamorphosis of river systems in mid-latitude regions experiencing conditions of rapid global warming.

Keywords: Paleocene-Eocene Thermal Maximum; PETM; fluvial channel; alluvial; fluvial architecture; global warming.

Introduction

A brief episode of extreme global warming related to the release of isotopically light carbon into the Earth's oceans and atmosphere is recorded across the Paleocene-Eocene boundary (ca. 56 Ma; Kennett & Stott 1991; Koch et al. 1992; Charles et al., 2011). This event is variably referred to as Initial Eocene Thermal Maximum, Latest Paleocene Thermal Maximum, or Paleocene-Eocene Thermal Maximum (PETM), and is believed to have been characterized by a rise in global temperatures of 5º to 9º C in 10 kyr, followed by a gradual decline to pre-PETM values that took between 100 and 200 kyr (Kennett & Stott 1991; Zachos et al. 2003; 2006; Tripati & Elderfield 2005; Sluijs et al. 2006; McInerney & Wing 2011). The stratigraphic expression of the PETM is often recognized by a characteristic negative shift in $\delta^{13}C$ (carbon isotope excursion; CIE), detected in both marine and terrestrial strata at the Paleocene-Eocene boundary (Kennett & Stott

53 1991; Koch et al. 1992; McInerney & Wing 2011, and references therein), although recent evidence
54 suggests that a warming trend was already established before the time recorded in the CIE
55 (Secord et al. 2010; Bowen et al. 2015)
56 Recent research has concentrated on how the PETM global changes affected sediment routing
57 systems, through controls on weathering (e.g., Bolle & Adatte 2001, and references therein;
58 Dallanave et al. 2010; Dypvik et al. 2011), sediment-delivery processes and rates (e.g., Schmitz &
59 Pujalte 2003; Minelli et al. 2013), and type, distribution and characteristics of sedimentary sinks
60 (e.g., Schmitz & Pujalte 2007; Foreman et al. 2012; Foreman 2014). Research effort has also been
61 dedicated to assessing the impact of the PETM hyperthermal event on the geomorphic change of
62 terrestrial landscapes, as documented in the stratigraphic record. In particular, recent publications
63 provide insight into the sedimentary record of the PETM for some continental successions in which
64 the stratigraphic position of the PETM is readily identifiable (Foreman et al. 2012; Foreman 2014;
65 Kraus et al. 2015). At the PETM, continental environments may have variably been affected by the
66 controls exerted by climate change on the eustatic level (Sluijs et al. 2008), on regimes of water
67 and sediment discharge to the river systems, and on characteristics of catchments, floodplains,
68 and interfluves, which are all themselves related to a number of climatically controlled variables.
69 A sedimentary succession of predominantly continental origin in which the stratigraphic position of
70 the PETM-related CIE is well constrained is the Tremp Group of the Tremp-Graus Basin, Spanish
71 Pyrenees (Schmitz & Pujalte 2003; 2007; Pujalte et al. 2014). Stratigraphic changes observed in
72 this succession across the CIE have been interpreted in terms of responses of river systems to the
73 PETM (Schmitz & Pujalte 2007).
74 Building upon previous studies, the aim of this work is to assess changes in sedimentary
75 architecture through the PETM in the Tremp Group, based on results from original facies and
76 architectural-element analyses, with the scope to better understand the response of the alluvial
77 landscapes to the hyperthermal event.

78 The analysed features are considered to reflect – in part – the geomorphic organization and
79 processes of the fluvial system at time of deposition. Lithofacies and associations thereof are
80 indicative of different processes, including primary depositional processes (e.g., deposition in
81 upper versus lower flow-regime conditions), and sub-environments (e.g., channel versus
82 overbank), respectively. Furthermore, architectural features of sedimentary bodies, such as the
83 geometry and nature of external and internal bounding surfaces and the relative spatial
84 arrangement of these bodies, bear a record of the original geomorphology of the depositional
85 systems. They relate landform types, their modes and rates of evolution, and their genetic
86 relationships, although not always in a straightforward manner (cf. Bridge 2003; and references
87 therein). On the basis of observations of the depositional architecture, inferences are here made
88 about the geomorphic change in alluvial landscapes associated with the PETM.
89 The specific objectives of this study are: (i) to provide a quantitative description of changes in
90 sedimentary architecture across the Paleocene-Eocene boundary in the Tremp Group, particularly
91 as documented over a km-scale strike-oriented transect; (ii) to discuss the significance of these
92 changes in terms of interpreted variations in geomorphic processes, landforms and associated
93 drivers.
94

95 ## Geological setting

96 The Pyrenees are an asymmetrical chain of mountains composed of doubly vergent thrust wedges
97 that formed in response to the collision between the Iberian and the European plates, during the
98 late Cretaceous to early Miocene (Puigdefàbregas & Souquet 1986; Vergés et al. 1995). The
99 south-central Pyrenees (Spain) consist of a fold-and-thrust belt divided into three imbricate west-
100 trending thrust sheets, which are referred to as the Bóixols, Montsec and Sierras Marginales, from
101 north to south, respectively (Burbank et al. 1992; figure 1A). Foreland basins developed on the
102 front of these thin-skinned thrust sheets. In the early Paleogene, one of these basins, the Tremp-
103 Graus Basin, evolved as a piggy-back basin (*sensu* Ori & Friend 1984) on top of the Montsec

thrust sheet, south of the Bóixols thrust (Eichenseer & Luterbacher 1992; Puigdefàbregas et al. 1992; Luterbacher 1998). The timing of thrust activity is reflected in the southward piggy-back propagation and dictates depocentre migration. The Bóixols thrust sheet was emplaced during the Late Cretaceous (Berástegui et al. 1990; Bond & McClay 1995; Fernández et al. 2012). Before the Paleocene-Eocene boundary, sedimentation in the Tremp-Graus Basin was contemporaneous with the incipient propagation of the Montsec thrust, although most of the activity of this lineament took place in the early Eocene (Williams 1985; Farrell et al. 1987; Puigdefàbregas et al. 1992; Sinclair et al. 2005; Fernández et al. 2012). At these times, the northern part of the Tremp-Graus Basin was being affected by the activity of underlying blind thrusts (Eichenseer & Luterbacher 1992; Luterbacher 1998). The Montsec frontal ramp and Bóixols thrust likely determined a basin physiography characterized by a steeper northern margin and a gentler southern one. The basin displayed a WNW-oriented axis, parallel to the orogen, and the drainage was consistently towards the Bay of Biscay to the west (Plaziat 1981; Cuevas 1992; Vergés & Burbank 1996; Whitchurch et al. 2011; figure 1).

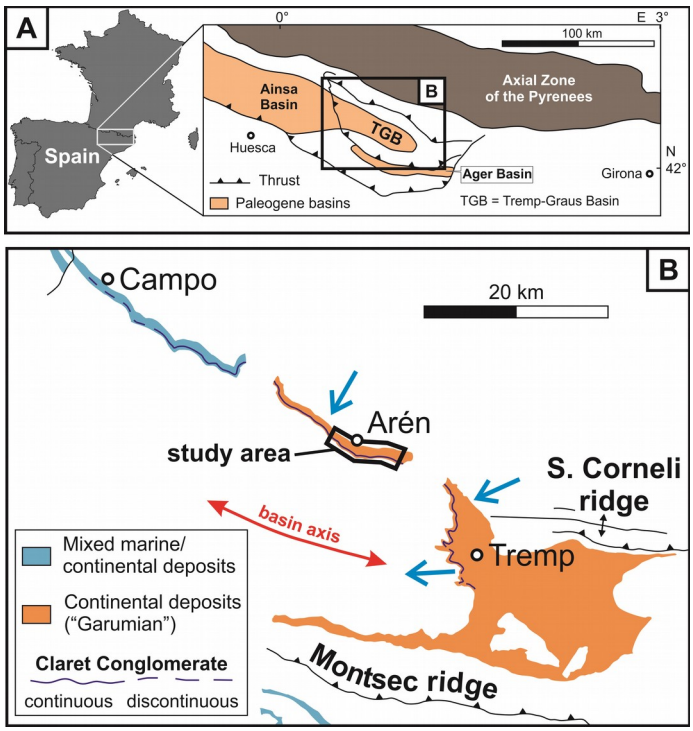

120 **Figure 1:** A) Location of the Tremp-Graus Basin in the structural setting of the southern Pyrenees. B)
121 Location of the study area on outcrop map of the early Paleogene deposits of the Tremp-Graus Basin. The
122 arrows indicate general drainage directions. The trace of the Claret Conglomerate marks the position of the
123 PETM. Modified after Pujalte et al. (2014).
124
125 Successions of late Paleocene-earliest Eocene age comprise siliciclastic and carbonate strata that
126 interfinger laterally and alternate vertically, and are interpreted to be of shallow-marine and
127 continental origin. A suite of continental and paralic clastic deposits that takes the informal name of
128 "Garumnian" is attributed to the Tremp Group, which is composed of the Thanetian to Ilerdian age
129 Esplugafreda and Claret formations (Cuevas 1992; Rosell et al. 2001; Pujalte & Schmitz 2005;
130 figure 2). The Esplugafreda Formation is 165-350 m thick, and largely consists of red mudstones
131 with intercalated arenaceous to conglomeratic bodies and evaporites of local occurrence, which
132 are interpreted to have accumulated in continental settings (Cuevas 1992; Dreyer 1993; Rosell et
133 al. 2001; Pujalte & Schmitz 2005; Pujalte et al. 2014, and references therein). A prominent erosive
134 surface, related to the incision of a network of lowstand valleys, defines the boundary between the

Esplugafreda and Claret formations (Pujalte et al. 2014). The Claret Formation is 10 to 70 m thick, and is composed of a varied suite of mudstones, sandstones, and conglomerates, with local gypsum accumulations, which are interpreted to have deposited in terrestrial to paralic settings (Pujalte & Schmitz 2005; Pujalte et al. 2014). Pujalte et al. (2014) describe five informal members within the eastern domain of the Claret Formation (cf. Baceta et al. 2011): member 1 consists of the infill of the basal valleys; member 2 consists of a dominantly conglomeratic unit (Claret Conglomerate); member 3 consists of yellowish pedogenized silty mudstones with intercalated sandstone bodies; member 4 is a gypsiferous unit; member 5 is mostly composed of red mudstone. The top of the Claret Formation is marked by a conformable contact with transgressive marine limestones above. Overall, the terrestrial deposits of the Garumnian strata record sedimentation in alluvial environments bordering ephemeral lakes and shallow seas; sedimentary bodies identified in the succession are interpreted as preserved geomorphic features such as channels, mid-channel bars, levees, crevasse splays, terminal frontal splays (Dreyer 1993; Schmitz & Pujalte 2007; Pujalte et al. 2014). Some of the sand-prone and conglomeratic bodies in this succession are interpreted by Mutti et al. (1996; 2000) as the preserved product of flood-dominated deposition at the termini of alluvial channels in shallow lakes. Garumnian outcrops indicate southward to westward alluvial drainage, from the structural reliefs in the north-east of the basin (Cuevas 1992; Vergés & Burbank 1996; Rosell et al. 2001; Pujalte et al. 2014). During the Paleocene, the Garumnian streams had their major source of sediment in catchments draining Variscan and Cadomian plutons of the Axial Zone of both the central and eastern Pyrenees, which were being exhumed at a rate of ca. 0.5 km/Myr (Whitchurch et al. 2011; Filleaudeau et al. 2012). These northern catchments were partly hosted in the advancing upland thrust sheets (Rosell et al. 2001). Carbonate clasts of lower and upper Cretaceous affinity are abundant in north-easterly sourced Garumnian sandstones and conglomerates, and are related to source rocks uplifted 10 to 20 km north of present-day outcrops (Schmitz & Pujalte 2007; cf. Teixel & Muñoz 2000; Gómez-Gras et al. 2016). The Montsec thrust sheet to the south represented only a minor source of

161 sediment for the Tremp-Graus Basin in the early Eocene (Williams & Fischer 1984; Williams 1985).
162 The clay-mineral composition of Garumnian palaeosols (Schmitz & Pujalte 2003) and of correlative
163 deep-marine deposits (Schmitz et al. 2001) is characterized by an increase in kaolinite content
164 recorded at the PETM, which is interpreted as related to enhanced rates of upland erosion that
165 mobilized buried kaolinite-rich Mesozoic sediments (Schmitz et al. 2001).
166
167

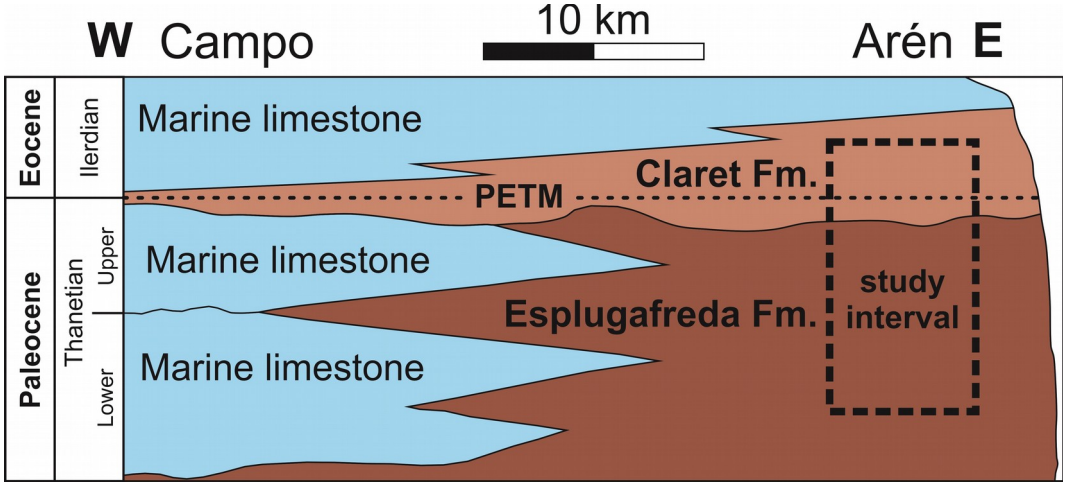

168 **Figure 2:** simplified stratigraphic scheme of the early Paleogene Garumnian along an east-west transect of
169 the Tremp-Graus Basin, between Campo and Arén. The stratigraphic coverage of the dataset is reported.
170 Modified after Pujalte et al. (2014).
171
172 In the Paleocene, the Tremp-Graus Basin, which connected westward to the sea, was subject to
173 relative sea-level fluctuations of various orders (Rasser et al. 2005), the stratigraphic record of
174 which is in part reflected in the sequence stratigraphic organization of the succession, as recorded
175 in the Campo, Navarri and Serraduy sequences of Luterbacher et al. (1991) (cf. Eichenseer &
176 Luterbacher 1992; Payros et al. 2000; Minelli et al. 2013). In the area where Garumnian deposits
177 crop out, two main marine transgressions occurred in the early and late Thanetian. A widespread
178 regression occurred in the latest Thanetian is expressed as the boundary between the
179 Esplugafreda and Claret formations. This was followed by a major transgression during the early

Ilerdian (Rasser et al. 2005; Pujalte et al. 2014). In the Garumian domain, one of the pre-PETM valley fills of the member 1 of Pujalte et al. (2014) contains co-occurring charophyte oogonia, small benthic foraminifera, rare gastropods and *Ophiomorpha* burrows, which collectively indicate fresh to brackish salinity (Pujalte et al. 2014). The PETM, which was associated with a period of eustatic rise (Miller et al. 2005; Sluijs et al. 2008), coincided with an interval of the early Ilerdian relative sea-level rise (Pujalte et al. 2014). However, despite the development of an overall early Ilerdian transgressive phase, conditions of depositional regression are observed for the PETM interval, supposedly in relation to a climate-driven increase in clastic supply (Minelli et al. 2013; Pujalte et al. 2014).

At the PETM, the Tremp-Graus Basin was situated at a palaeolatitude of ca. 35°N (Butterlin et al. 1993), which corresponds with the position of present-day subtropical high-pressure cells. Pedogenized mudstones of the pre-PETM Esplugafreda Formation are dominantly red and purple, display colour banding and mottling, contain well-developed 0.5 to 2 m-thick Bk horizons with abundant cm-sized calcite nodules, are typically rich in Microcodium, and locally show vertic features; several gypsiferous intervals also occur in the upper half of the Esplugafreda Formation (Eichenseer & Luterbacher 1992; Dreyer 1993; Schmitz & Pujalte 2003; 2007). Overall, these observations are interpreted as indicative of a well-drained substrate in a semiarid to arid palaeoenvironment (Eichenseer & Luterbacher 1992; Schmitz & Pujalte 2007), which is thought to have been associated with dominantly ephemeral discharge regimes (Dreyer 1993). Based on independent evidence provided by clay mineral associations, Garumnian palaeosols have been interpreted as indicative of a hot climate with seasonal rainfall for the early Thanetian (Arostegi et al. 2011). The PETM interval in the Claret Formation is characterized by palaeosols with colour varying from reddish-brown, grey-purple to yellowish, and by high calcite content and dispersed carbonate nodules, indicative of a cumulate soil profile (*sensu* Wright & Marriott 1996; Baceta et al. 2011). A semiarid climate and variations from well to moderately or poorly drained conditions are inferred on the basis of these characteristics (Schmitz & Pujalte 2007; Dawson et al. 2014). The

development of poorly-drained, reducing conditions in relation to a general phreatic rise is in accord with the fact that portions of the Claret Conglomerate are locally abundant in coaly fragments, found in grey mudstones and silty sandstones in the Arén area (cf. Dreyer 1993; Schmitz & Pujalte 2003). However, carbonaceous material and grey palaeosol colours are also observed in parts of the member 1 of the Claret Formation predating the CIE (Dawson et al. 2014; original field observations), suggesting that if these characteristics recorded an overall wetting trend (cf. Schmitz & Pujalte 2003), this would have been established before the PETM. An increase in precipitation amounts and seasonality at the PETM has been postulated for the broader region on the basis of numerical simulations, which point to enhanced moisture transport from the Tethys, particularly in summer months (Winguth et al. 2010). Gypsum accumulations of the member 4 of the Claret Formation, supposedly contemporaneous with the PETM recovery phase (Domingo et al. 2009; Pujalte et al. 2014), have been related to deposition in saline lakes and surrounding mud flats, indicating that a relatively arid climate was established at that stage (García Veigas 1997; Pujalte et al. 2014).

Tropical forests dominated the Iberian region during the late Paleocene-early Eocene (Barrón et al. 2010). In the Garumnian strata, rhizoliths are observed throughout the succession in muddy palaeosols, including the yellowish palaeosol of PETM age (Pujalte et al. 2014). Correlative deep-marine deposits in the down-dip Basque Basin display a turnover in the composition of the non-marine palynomorph assemblage at the PETM, suggesting that in the nearby continental areas pre-PETM permanent gymnosperm forests were replaced by a seasonal cover of angiosperms and ferns and allies, which grew during rainy episodes (Schmitz et al. 2001).

A chronological framework for the Garumnian is provided by data on the distribution of charophytes (Feist & Colombo 1983), palynomorphs (Médus & Colombo 1991) and mammal teeth (Lopéz-Martínez & Peláez-Campomanes 1999). For the Thanetian, a further chronological constraint is provided by tentative stratigraphic correlations with marine strata (e.g., Luterbacher et al. 1991). The identification of the PETM is aided by recognition of the characteristic negative carbon isotope

232 excursion (CIE), which is recorded in palaeosol carbonates and organic matter contained in the
233 Claret Formation. In the Arén area, a magnetostratigraphic section spanning the CIE records only
234 reverse polarities (Lopéz-Martínez et al. 2006). Although discrepancies exist regarding the precise
235 position of the PETM onset relative to the Claret Conglomerate (Schmitz & Pujalte 2007; Domingo
236 et al. 2009; Manners et al. 2013; 2014; Adatte et al. 2014; Pujalte et al. 2014), the CIE can be
237 identified in the members 2 and 3 of Pujalte et al. (2014). Although the lowest values of $\delta^{13}C$ are
238 recognized within the member 3 by Adatte et al. (2014), these authors interpret this particular $\delta^{13}C$
239 excursion as the preserved signal of the subsequent Eocene Thermal Maximum 2, and argue that
240 the position of the record of the onset of the PETM is ca. 15 m below the top of the Claret
241 Conglomerate. However, this interpretation contradicts existing stratigraphic constraints (cf. Pujalte
242 et al. 2009, and references therein).
243
244 **Methods and data**
245 Sedimentological data have been acquired from a ca. 7-km-long, near-strike-oriented transect from
246 the Arén area (figure 1). Facies analysis and architectural-element analysis of fluvial deposits have
247 been undertaken, with particular attention to fluvial channel deposits (cf. Dreyer 1993). For
248 measured vertical sections and architectural panels, lithofacies have been described and classified
249 in terms of textural and structural properties; Munsell colours were recorded for pedogenically
250 modified mudstones. Palaeocurrent directions (N = 536) have been determined for individual
251 lithofacies from cross bedding, cross lamination, clast imbrication and sole marks. The external
252 geometry of some sedimentary units (depositional and architectural elements; see below) has
253 been quantified through collection of data on maximum thickness and width of each unit. The
254 values of width of the bodies are apparent; whereas the orientation of the outcrop transect is
255 relatively constant and approximately directed along strike; stratigraphic changes might still reflect
256 temporal or local variations in drainage direction. The internal stratal geometries of sand-prone and
257 conglomeratic lithosomes, and the nature and hierarchical arrangement of associated bounding

surfaces have also been described. The spatial relationships between sedimentary units have been recorded. Data on maximum extraclast size (N = 91) and cross-set thickness (N = 132) have been recorded for several architectural elements. The sedimentological data have been collated into a relational database that permits the digitization of the sedimentary architecture of fluvial depositional systems (the Fluvial Architecture Knowledge Transfer System, FAKTS; Colombera et al. 2012; 2013). The classification schemes employed in FAKTS have been adopted, which apply to sedimentary units that belong to three scales of observation and are termed ‘depositional elements’, ‘architectural elements’ and ‘facies units’, in order of descending scale. On the basis of their facies associations and architectural characteristics, the sedimentary bodies of the Tremp Group have been classified according to interpretative depositional- and architectural-element types. Depositional elements are large-scale sedimentary bodies classified as ‘channel-complex’ or ‘floodplain’ elements on the basis of the interpreted origin of their deposits, and the subdivision of the stratigraphy in these units is partly based on geometrical rules (cf. Colombera et al. 2012; 2013). A channel complex is a discrete channelized body, and does not possess a particular genetic or palaeo-geomorphic significance: for example, a channel complex could correspond to the preserved product of a channel belt, of a channel, to a portion of valley fill, or to a compound amalgamated multi-storey body.

Architectural elements represent sedimentary bodies with characteristic facies associations and architectural properties that make them interpretable as types of sub-environments, which generally have a distinctive geomorphic significance and commonly record the morphodynamic evolution of a particular landform. The attribution of a particular element type follows criteria based on the characters of their bounding surfaces, their geometry, scale, internal organization, and – in some instances – their relationships with other elements (cf. Miall 1996; Colombera et al. 2013). Architectural-element types include aggradational channel fills (either active or abandoned at the time of filling) and barforms (classified on dominant direction of accretion: lateral, downstream). Facies units represent packages with sub-bed-scale resolution characterized by given textural and

structural properties on which they are classified. Facies units are delimited by bounding surfaces that mark a change in lithofacies, a major change in palaeocurrent, or erosional contacts (cf. 2nd-order surfaces of Miall, 1996; see Colombera et al. 2013). The adopted classification scheme of facies-unit types extends the scheme of Miall (1996). Facies types recognized in channel deposits of the study succession are summarized in table 1; photographic examples of the main lithofacies of channel deposits are presented in figure 3.

291

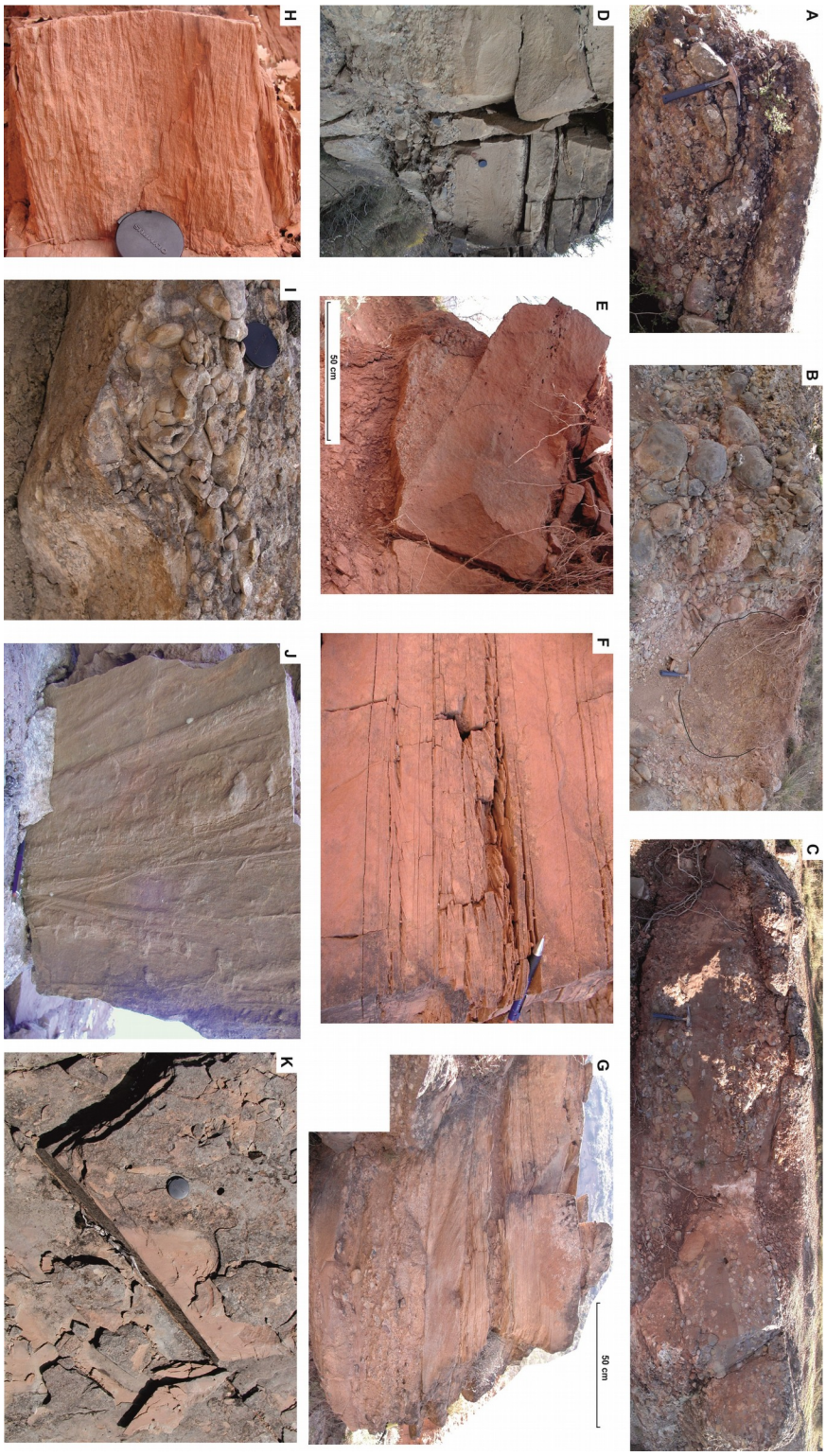

292 **Figure 3:** selected field photographs of lithofacies forming channel deposits in the Esplugafreda and Claret

293 formations. (A) Planar cross-stratified and crudely horizontally bedded conglomerates (syn-PETM Claret

Conglomerate). (B) Clast-supported, massive boulder conglomerate; a boulder-sized intraclast that exceeds 1 m in diameter is outlined in black (deposit from member 2 or uppermost member 1 of the Claret Formation based on attribution of Pujalte et al., 2014). (C) Interbedded crudely horizontally bedded and cross-stratified conglomerates and low-angle cross-stratified sandstones (Claret Conglomerate). (D) Crudely bedded cobble conglomerates and massive sandstones (pre-PETM member 1 of the Claret Formation). (E) Crudely bedded pebble conglomerates and massive sandstones (pre-PETM Esplugafreda Formation). (F) Interbedded planar horizontally bedded and ripple cross-laminated sandstones (Esplugafreda Formation). (G) Facies forming an aggradational ribbon channel fill of the Esplugafreda Formation, comprising beds of interbedded horizontally crudely bedded conglomerates and massive sandstones, planar, trough and low-angle cross-stratified sandstones, and planar horizontally bedded sandstones; view oriented along mean palaeoflow direction. (H) Climbing ripple cross-laminated sandstone bed (Esplugafreda Formation). (I) Gutter cast from the base of a channelized unit (Claret Conglomerate). (J) Groove casts from the base of a sandstone bed (Esplugafreda Formation). (K) Plan view of a planar horizontally bedded sandstone with primary current lineation (Esplugafreda Formation). The hammer is 35 cm long; the lens cap is 5 cm in diameter; the pen is 14 cm long.

Table 1: facies types recognized in channel deposits of the study succession, based on the scheme of Miall (1996). These facies are adopted in this work to describe channel deposits only, in the studied succession.

Code	Characteristics
Gcm	Clast-supported, massive conglomerate
Gh	Clast-supported, horizontally- or crudely-bedded conglomerate; possibly imbricated
Gt	Trough cross-stratified conglomerate
Gp	Planar cross-stratified conglomerate
St	Trough cross-stratified sandstone
Sp	Planar cross-stratified sandstone
Sr	Current ripple cross-laminated sandstone
Sh	Horizontally bedded sandstone
Sl	Low-angle (<15˚) cross-bedded sandstone
Sm	Massive sandstone; possibly locally graded or faintly laminated
Fl	Interlaminated very-fine sandstone, siltstone and mudstone, locally with thin cross-laminated sandstone lenses

Fsm	Massive or laminated siltstone and mudstone

Sedimentological change at the PETM is analysed quantitatively. Features that are compared include the geometry and proportion of channel complexes, architectural elements and facies units. Channel complexes are not related to any given geomorphic form by definition; thus, interpretation of changes in channel-complex properties in terms of geomorphic change can only be made in consideration of changes observed at the scale of the architectural elements. Estimation of the bankfull depth of formative channels is commonly attempted from measurement of the geometrical properties of preserved deposits (cf. Bridge & Tye 2000; Mohrig et al. 2000; Leclair & Bridge 2001; Bhattacharya & Tye 2004; Hajek & Heller 2012; Lunt et al. 2013). The thickness of barforms and channel fills provides a proxy for the maximum bankfull depth of their formative channels (cf. Bridge & Tye 2000; Mohrig et al. 2000; Bhattacharya & Tye 2004). However, such estimates can be affected by issues of partial preservation, related to erosional truncation of portions of sedimentary units, and compaction. Furthermore, the hydraulic geometry of a channel as inferred from preserved deposits is not necessarily indicative of the water discharge associated with a river system, as a multi-thread river pattern (braided, anastomosing), or local changes in drainage pattern (distributary as opposed to tributary) may have developed. Additional uncertainty is associated with the correct interpretation of architectural units as preserved geomorphic elements. For example, overestimates of channel depth could arise from the misinterpretation of scour fills (e.g., confluence scours) as channel fills (Miall & Jones 2003), whereas underestimates of bankfull depth could arise from the misinterpretation of the upper portions of barforms as overbank deposits (Latrubesse 2015).

Two-sample t-tests were performed to assess whether the differences between architectural parameters (log-transformed to meet the requirements of normality and homoscedasticity) of syn-PETM and pre-PETM deposits were statistically significant. Variations in the relative proportions

337 and grainsize of lithofacies types are employed to infer variations in the relative dominance of
338 different depositional processes, such as the importance of bed-load, suspended-load or mass-
339 flow deposition, or of upper versus lower flow-regime conditions. All results carry the fundamental
340 uncertainty that is inherent in the methods of facies and architectural analysis, as applied to the
341 rock record to infer past depositional and geomorphic processes.
342 Data on syn-PETM strata of the members 2 and 3 (Pujalte et al. 2014) of the Claret Formation are
343 separately compared with corresponding data from the pre-PETM member 1 and Esplugafreda
344 Formation.
345 Overall, the dataset comprises of data on:
346 • 247 channel complexes;
347 • 123 interpreted architectural elements, of which 108 are barforms and channel-fills;
348 • 1,397 facies units contained in channel complexes.
349
350 **Results**
351 Variations in sedimentary architecture are evaluated quantitatively across the pre-PETM and syn-
352 PETM intervals of the Claret Formation, and also relative to the older Esplugafreda Formation as a
353 control of the importance of stratigraphic changes through the record of the PETM.
354 The pre-PETM interval of the Claret Formation (member 1) is recognized as the infill of lowstand
355 valleys (Baceta et al. 2011; Pujalte et al. 2014). Three discrete depression fills are recognized in
356 the study area by Pujalte et al. (2014), one of which, the easternmost, appears as the compound
357 infill of multiple coalescing depressions. The existence of the single westernmost depression, at
358 least in the extent mapped by Pujalte et al. (2014), is here disputed based on field evidence
359 consisting of surface correlations walked out on outcrop and traced on panoramic outcrop
360 photomosaics, aided by recognition of channel-body pinch-out positions and palaeosol intervals.
361 On this basis, it can be suggested that at least part of the stratigraphic interval indicated as
362 ‘western depression’ by Pujalte et al. (2014) may constitute the preserved expression of an

363 interfluve – rather than a valley – rich in channel deposits that are more ancient than the member 1
364 of the Claret Formation. This has implications concerning the stratigraphic attribution of deposits
365 contained in this interval, which would predate the time of incision of the valleys at the base of the
366 Claret Formation. However, in view of the current uncertainty and to avoid confusion with the
367 existing stratigraphic scheme, these deposits are assigned to the member 1 of the Claret
368 Formation following the usage of Pujalte et al. (2014).
369 In each of the three intervals considered, fluvial channel complexes are recognized. Each channel
370 complex represents a discrete channelized unit, made of channel deposits (figure 4). The studied
371 channel complexes are interpreted to relate to a range of formative processes and have variable
372 geomorphic significance. For example, in the Esplugafreda Formation channel bodies are locally
373 seen to form the complete aggradational infill of depressions, whereas other occurrences might
374 just represent simple isolated channel fills, channel belts or amalgamated channel belts, locally
375 positioned on valley floors in the member 1 of the Claret Formation.
376

Figure 4: selected field photographs documenting aspects of the large-scale sedimentary architecture of the Esplugafreda and Claret formations. (A) Photopanel with view of the stratigraphy for the study interval on the southern hillside of the Esplugafreda valley. The member 1 of the Claret Formation in this area forms a palaeovalley fill, the 'central depression' of Pujalte et al. (2014). The stratigraphy dips into the hillside. (B) Detailed view of the sedimentary architecture seen on the slope corresponding to the western side of the photopanel in part A. The bases of cut-and-fill units from the Esplugafreda Formation are outlined in black.

The view is rotated to the approximate palaeo-horizontal. (C) Vertically stacked sand-prone channel bodies; their left-hand margins are outlined in black. (D) Conglomeratic bodies interbedded with red mudstones, seen across the transition between inferred pre- and syn-PETM deposits. The topmost conglomeratic unit corresponds to the syn-PETM Claret Conglomerate (black arrow). Some of the underlying cut-and-fill conglomeratic units are stratigraphically positioned in the pre-PETM member 1 of the Claret Formation according to the scheme of Pujalte et al. (2014), supposedly next to the western margin of the 'west depression' of the Arén area. In this area, surfaces that could unambiguously be identified as palaeovalley margins were not observed, and the variety of palaeosol colours seen in the member 1 further to the east is lacking. (E) Photopanel with view of the stratigraphy for the study interval, on a hillside of a ravine 1 km southwest of Arén. The lower section consists of deposits of the Esplugafreda Formation; the cliff is topped by deposits of the Claret Conglomerate (black arrow); the lower ledge-forming conglomeratic bodies contained in the upper section below the Claret Conglomerate are assigned to the member 1 of the Claret Formation ('western depression') of Pujalte et al. (2014). The asterisk marks the position of the channel body in figure 4F. (F) sand-prone channel body; the channel-body margins, which are expressed as erosional cuts of pedogenically modified mudstones, and its base are outlined in black.

At a lower scale of observation, different types of architectural elements are documented in the channel complexes. These sedimentary bodies are interpreted as the product of infill of fluvial channels (figure 5) and of accretion of barforms of different types (figure 6).

Two main types of barforms are identified based on lithological and architectural characteristics. In some cases inferences of the direction of accretion of these bars are uncertain, being hampered by the limited occurrence of palaeocurrent indicators and/or by the nature of the outcrop exposures. Conglomeratic barforms that appear to be dominantly accreting downstream (figure 6A-C) are seen in all three stratigraphic intervals. Some of these deposits are interpretable as bank-attached bars because of their adjacency to preserved cut-banks. Barforms that are variably gravel-, sand-, and silt-prone and that locally demonstrate lateral accretion are recognized in the syn-PETM

412 interval of the Claret Formation, in accordance with observations by Schmitz & Pujalte (2007).
413 Characteristic differences in facies architecture are seen between the architectural-element types
414 that compose the channel complexes (figure 7).
415

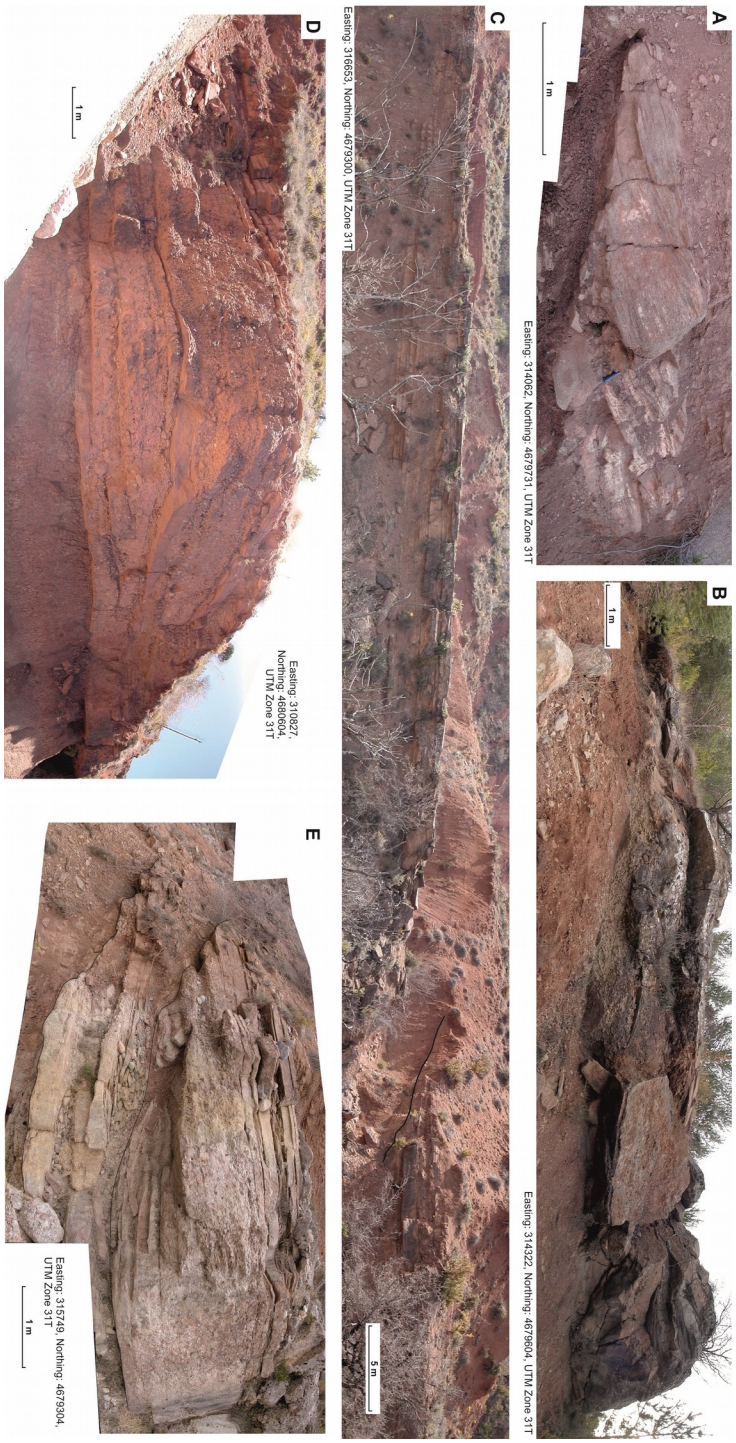

Figure 5: selected field photographs of the sedimentary architecture of aggradational channel fills. (A) Detail of the margin of a sand-prone channel-fill (CH) architectural element. (B) Detail of a channel-body margin from the Claret Conglomerate interval. The channel-body top is contained within grey mudstones of the syn-PETM member 2 of the Claret Formation; the base of the body is incised into red mudstones of the member

1. The mean palaeoflow is oriented obliquely into the outcrop. (C) Aggradational ribbon channel fill, seen to be cut both perpendicularly (to the right) and longitudinally (to the left) relative to its axis; the left-hand channel-fill margin is outlined in black. (D) Dominantly conglomeratic channel fill, with overall fining-upward trend. (E) Vertically stacked channel fills from the pre-PETM member 1 of the Claret Formation. The bases of the channel bodies are outlined in black. The mean palaeoflow is oriented approximately into the outcrop.

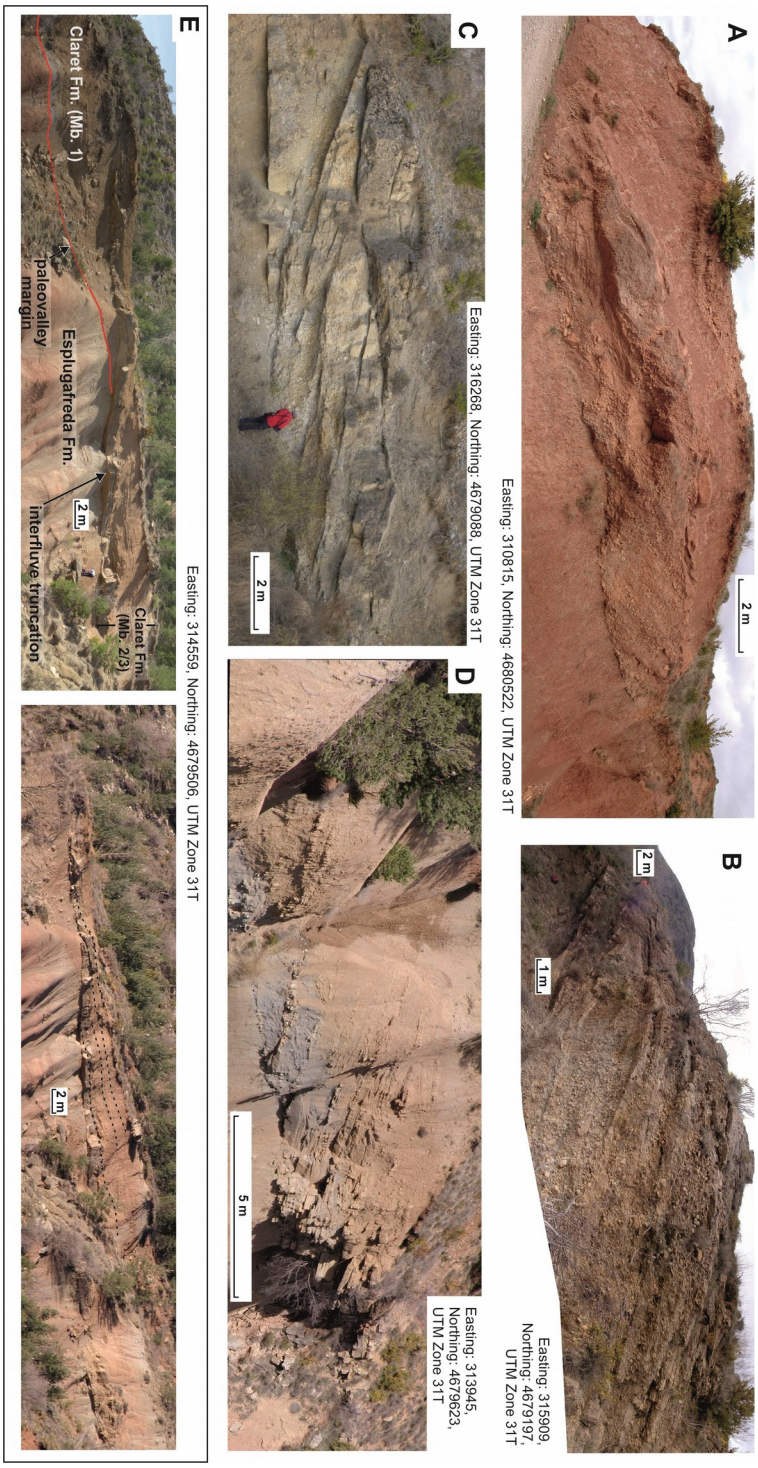

428 **Figure 6:** selected field photographs of the sedimentary architecture of barforms. (A) Gravelly barform
429 embedded in red palaeosols from the uppermost part of the Esplugafreda Formation; see figure 2 of Mutti et
430 al. (2000) for alternative interpretation. (B) Oblique view of a multistorey channel body from the syn-PETM

Claret Conglomerate interval. The central part of the channel body consists of a package of clinothems made of interbedded sandstones and conglomerates that is seen to record accretion at low-angle with the palaeoflow direction. The mean palaeoflow is oriented obliquely into the outcrop and to the right-hand side. (C) Multistorey channel body from the syn-PETM Claret Conglomerate interval. The central part of the channel body consists of a package with clinoforms marked by interbedded sandstones and conglomerates; this package is seen to record accretion at low-angle with the palaeoflow. The mean palaeoflow is oriented to the right-hand side. (D) Package of sandy clinothems from the syn-PETM interval of the Claret Formation (members 2 and 3). The buff-coloured upper portion of the body corresponds to the member 3 ("yellowish soils" of Pujalte et al., 2014, and references therein). (E) Outcrop expression of the relationships between the Esplugafreda Formation and the members 1 and 2 of the Claret Formation; this is the same outcrop documented in the Supplementary figure 3C of Schmitz & Pujalte (2007) and in the supplementary figure 3B of Pujalte et al. (2014). The base of the Claret Formation, consisting in the palaeovalley wall interpreted by Pujalte et al. (2014), is traced in red. Thus, the syn-PETM part of the Claret Formation is seen to rest on both the valley fill and the associated interfluve, which consists of deposits of the Esplugafreda Formation and appears as sharply truncated by deposits that mark the onset of the PETM. The ledge-forming conglomeratic unit attributed to the Claret Conglomerate may be interpreted as a basal lag; the overlying deposits consist of massive silty very fine sandstones alternating with locally pebbly, massive or faintly laminated, fine to medium sandstones; these beds are possibly genetically related to the basal lag, on which they appear to be downlapping, rather than onlapping (cf. Schmitz & Pujalte 2007 for alternative interpretations).

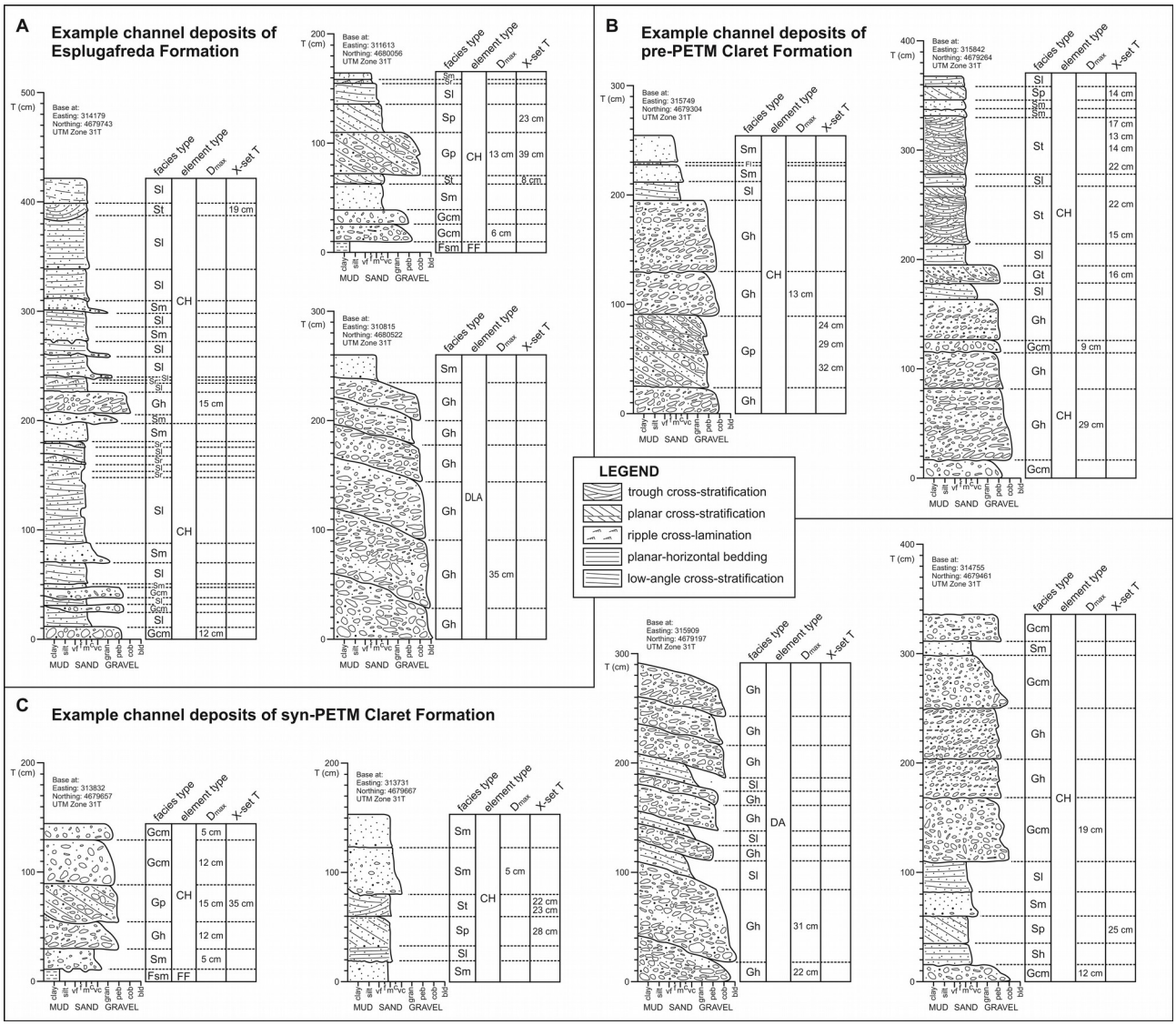

452 **Figure 7:** vertical logged sections of selected examples of in-channel architectural elements from different
453 stratigraphic intervals: Esplugafreda Formation (A), member 1 of the Claret Formation (B), and members 2
454 and 3 of the Claret Formation (C). These examples have been chosen to illustrate the variability in facies
455 organization seen in channel deposits of the studied succession of the Tremp-Graus Basin. The data
456 contained in quantified form in the article refers to a total of 87 architectural elements, characterized through
457 field data collection. The represented logs do not comprise all the qualitative information recorded in the field,
458 but only what is directly made use of in this article and presented in quantified form therein. See table 1 for
459 explanation of lithofacies codes in the 'facies type' column.
460

Descriptive statistics of the geometry of channel complexes from the different intervals are summarized in tables 2 and 3, and in figure 8. Channel complexes from the members 2 and 3 (N = 33) return higher values of mean, median and maximum axial thickness, compared to channel complexes from the Esplugafreda Formation (N = 186) and from the palaeovalley fills of the member 1 of the Claret Formation (N = 28). The difference in mean channel-complex thickness seen between the pre- and syn-PETM intervals is statistically significant at the 0.01 level if determined for the entire succession (two sample t-test of log-transformed data, T=-4.16, df=45, P=0.000), but only at the 0.1 level if evaluated across the members of the Claret Formation only (two sample t-test of log-transformed data, T=-1.71, df=58, P=0.093). The difference in mean channel-complex width seen between the pre- and syn-PETM intervals and determined for the entire succession is statistically significant at the 0.01 level (two sample t-test of log-transformed data, T=-4.79, df=9, P=0.001).

Table 2: descriptive statistics of channel-complex thickness for the study intervals of the Tremp-Graus Basin succession.

	Mean thickness (m)	Median thickness (m)	Maximum thickness (m)	Thickness standard deviation (m)	N
Esplugafreda Fm.	2.3	2.1	9.4	1.5	186
Mb. 1 Claret Fm.	2.7	2.7	5.0	1.1	28
Mb. 2/3 Claret Fm.	3.6	2.9	11.0	2.2	33

Table 3: descriptive statistics of channel-complex width for the pre- and syn-PETM intervals of the Tremp-Graus Basin succession. Widths are measured along a direction that approximates depositional strike, but might be apparent relative to the drainage direction of each channel complex.

	Mean width (m)	Median width (m)	Maximum width (m)	Width standard deviation (m)	N

Esplugafreda Fm. + Mb. 1 Claret Fm.	35.2	15.7	747.4	77.3	169
Mb. 2/3 Claret Fm.	484.0	352.0	1432.0	508.0	10

481

482

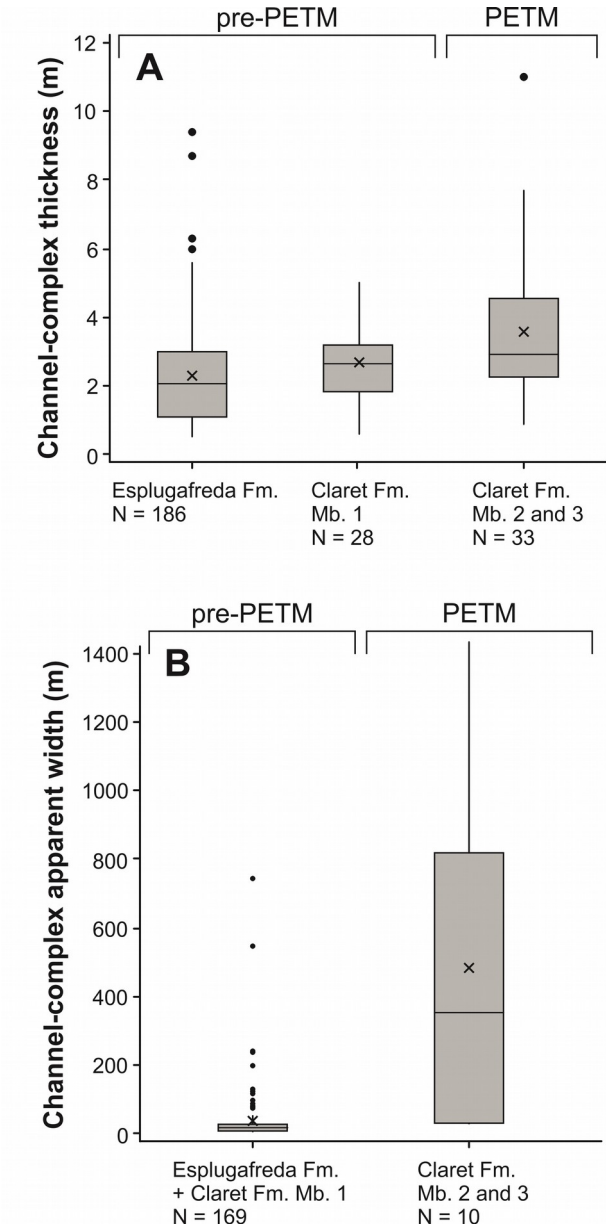

484 **Figure 8:** box plots that describe the distribution of channel-complex thickness (A) and apparent width (B) for
485 the stratigraphic intervals considered. Boxes represent interquartile ranges, horizontal bars within them
486 represent median values, crosses (x) represent mean values, and spots represent outliers.

487

488

489 Descriptive statistics of the geometry of architectural elements contained in channel complexes
490 and interpreted as channel fills or barforms, which are present in this succession as both laterally

and downstream accreting macroforms, are summarized in table 4 and figure 9. In-channel architectural elements from the syn-PETM members 2 and 3 of the Claret Formation (N = 31) return marginally higher values of mean and standard deviation of axial thickness, compared to elements from the Esplugafreda Formation (N = 45) and from the member 1 (N = 25). The difference in mean thickness for the channel fills and barforms of the pre- and syn-PETM intervals is not statistically significant (two sample t-test of log-transformed data, T=-0.82, df=50, P=0.416). A significant increase in standard deviation of channel-fill and barform thickness is seen across the pre- and syn-PETM members of the Claret Formation (Bonett's test, P=0.015; Bonett 2006). Whereas aggradational channel fills seem to dominate in the Esplugafreda Formation, over 20% of the studied in-channel architectural elements in the Claret Formation are classified as barforms: this is likely a conservative percentage, as the orientation of outcrop exposures in the Arén area commonly hinders recognition of accretion geometries.

Table 4: descriptive statistics of in-channel architectural-element (barform and channel fill) maximum thickness for the study intervals of the Tremp-Graus Basin succession.

	Mean thickness (m)	Median thickness (m)	Maximum thickness (m)	Thickness standard deviation (m)	N
Esplugafreda Fm.	2.1	2.0	5.6	1.1	45
Mb. 1 Claret Fm.	2.2	1.9	3.7	0.7	25
Mb. 2/3 Claret Fm.	2.4	1.9	6.5	1.4	31

Figure 9: box plots that describe the distribution of in-channel architectural-element thickness for different stratigraphic intervals of the Tremp-Graus Basin. Boxes represent interquartile ranges, horizontal bars within them represent median values, crosses (x) represent mean values, and spots represent outliers.

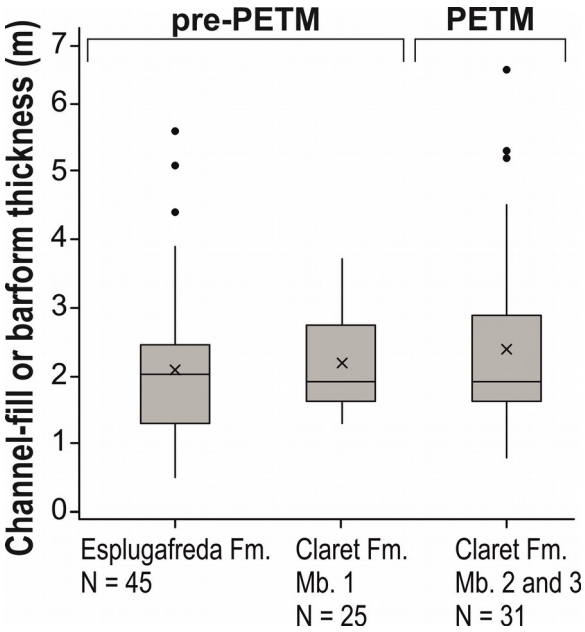

Information on the facies architecture of the channel complexes is obtained in the form of total proportions of different facies types in channel deposits, based on summed thicknesses, for the study intervals (figure 10). As compared to the Esplugafreda Formation, channel complexes from both the pre- and syn-PETM Claret Formation exhibit a larger proportion of gravelly deposits (70% versus 53%) and a smaller proportion of fine-grained deposits (2% versus 7%). In the Claret Formation, channel deposits in the syn-PETM interval display a higher proportion of conglomerates (73% versus 66%) compared to those in the pre-PETM member 1. A progressive increase (11% in the Esplugafreda Formation, to 23% in member 1, to 26% in members 2 and 3) in the proportion of cross-stratified units (Gt, Gp, St, Sp) and decrease (30% to 15% to 9%, respectively) in the proportion of plane-bedded or low-angle cross-stratified sandstones (Sh, Sl) are recorded through the three intervals. The decrease in the fraction of horizontally bedded sandstone is particularly significant across the Esplugafreda and Claret formations (28% to 4%). Through these intervals, an increase in the amount of massive sandstone in channel complexes is also recorded (3% to 8%); the proportion of massive sandstones that appear bioturbated shows modest change (12% to 14% of ‘Sm’ facies). Sandstones with soft-sediment deformation are notably absent from the sampled channel complexes.

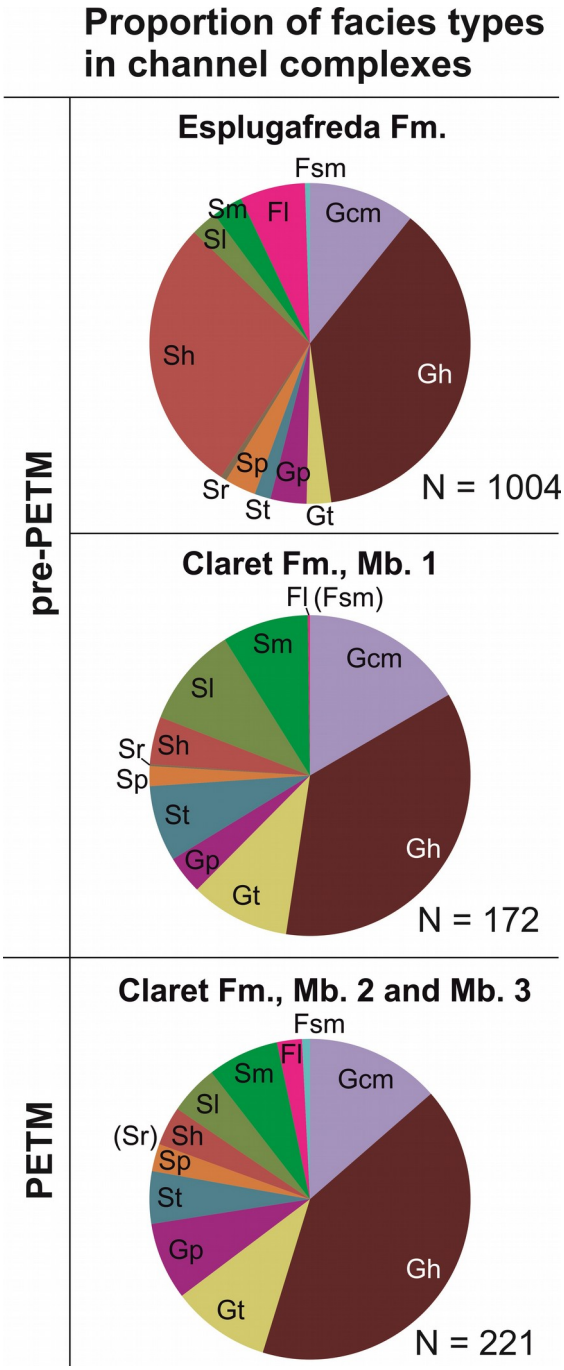

531 **Figure 10:** pie charts of the proportion of facies unit types in channel complexes from the stratigraphic
532 intervals considered.

533

534 Descriptive statistics of measured values of maximum extraclast size by architectural element is
535 reported in table 5 and figure 11. The largest extraclasts in architectural elements of the members

536 2 and 3 (N = 42) return values of central tendency and dispersion comparable with figures from the
537 Esplugafreda Formation (N = 21) and the member 1 of the Claret Formation (N = 28). Quantitative
538 data on intraclast size are lacking.

539

540 **Table 5:** descriptive statistics of maximum extra-clast size for in-channel architectural elements (channel fills, barforms)
541 for the studied intervals.

	extraclast D_{max} mean (cm)	extraclast D_{max} median (cm)	extraclast D_{max} maximum (cm)	extraclast D_{max} standard deviation (cm)	N
Esplugafreda Fm.	22.9	23.0	45	11.4	21
Mb. 1 Claret Fm.	25.0	20.0	59	13.8	28
Mb. 2/3 Claret Fm.	23.2	20.0	63	13.6	42

542

543

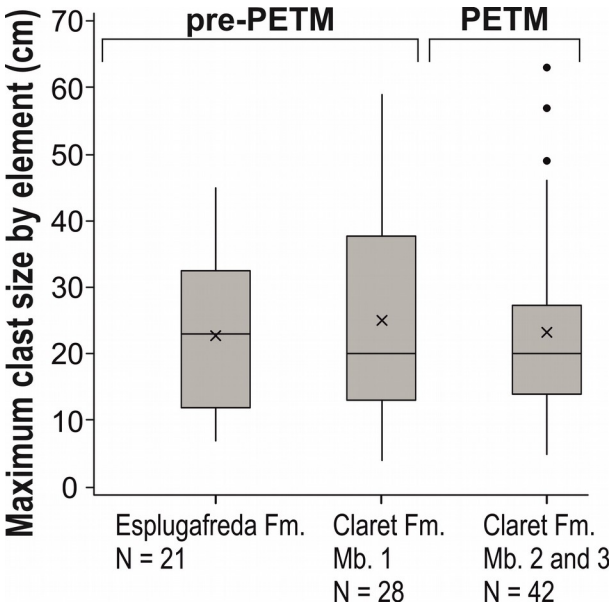

545 **Figure 11:** box plots of the distribution of maximum extra-clast size for in-channel architectural elements
546 (channel fills, barforms) for the studied stratigraphic intervals. Boxes represent interquartile ranges,
547 horizontal bars within them represent median values, crosses (x) represent mean values, and spots
548 represent outliers.

549

550 Descriptive statistics of cross-set thickness have been considered for medium-scale cross-bedded
551 conglomerates (Gp, Gt) and cross-bedded sandstones (Sp, St), and are reported in table 5 and
552 figure 12. Mean cross-set thickness is 19.1 cm, median cross-set thickness is 15 cm, and
553 maximum cross-set thickness is 68 cm (standard deviation = 13.1 cm). Cross-bedded sandstones
554 from the syn-PETM members 2 and 3 of the Claret Formation (N = 54) return higher values of
555 mean and median cross-set thickness than sandstones from the Esplugafreda Formation (N = 21)
556 and the member 1 of the Claret Formation (N = 24). The difference in mean cross-set thickness
557 seen in channel sandstones of the pre- and syn-PETM intervals is statistically significant (two
558 sample t-test of log-transformed data, T=-3.51, df=96, P=0.001).

559

560 **Table 6:** descriptive statistics of cross-set thickness for cross-stratified conglomerates (CGL) and sandstones (SST) in
561 channel deposits from the studied intervals.

		x-set thickness mean (cm)	x-set thickness median (cm)	x-set thickness maximum (cm)	x-set thickness standard deviation (cm)	N
CGL	Esplugafreda Fm.	43.4	45.0	56	11.6	5
	Mb. 1 Claret Fm.	33.9	31.5	66	12.8	10
	Mb. 2/3 Claret Fm.	39.6	32.5	75	15.6	18
SST	Esplugafreda Fm.	19.1	15.0	68	13.1	21
	Mb. 1 Claret Fm.	17.2	15.0	40	6.6	24
	Mb. 2/3 Claret Fm.	24.1	23.0	45	9.2	54

562

563

564

565 **Figure 12:** box plots of the distribution of cross-set thickness for cross-stratified sandstones and
566 conglomerates in channel deposits from the studied stratigraphic intervals. Boxes represent interquartile

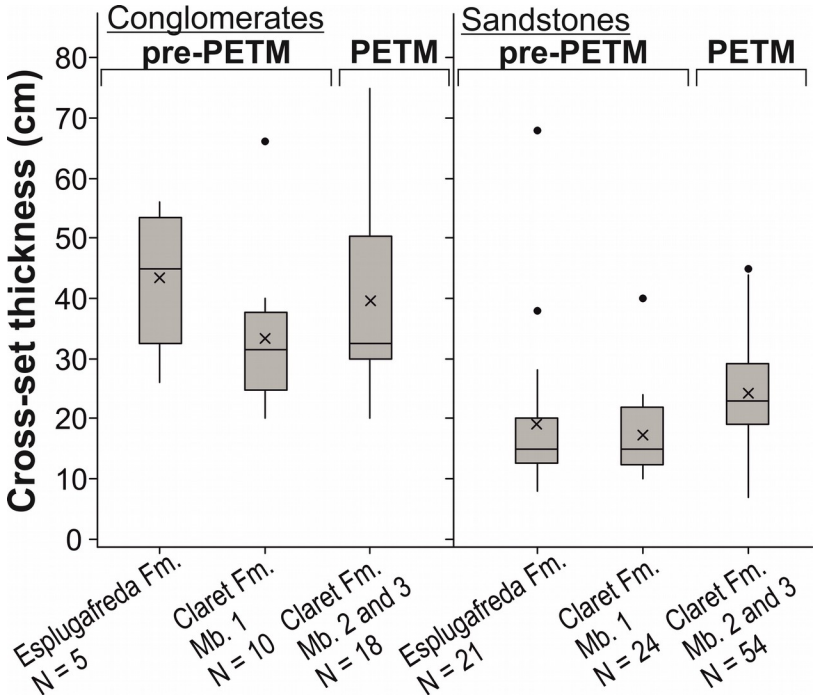

Discussion

Revisiting previous interpretations

An analysis of the significance of sedimentological change observed across the PETM in the Tremp-Graus Basin was made by Schmitz & Pujalte (2003; 2007), who also discussed the potential importance of tectonics and relative sea level. As noted by Schmitz & Pujalte (2007), the intervals that embody the onset and main phase of the PETM (i.e., the members 2 and 3 of the Claret Formation) are characterized in the Arén area by an overall higher proportion of channel deposits compared to underlying strata, and a significant reduction in channel-body density is observed vertically between the interval of members 2/3 and member 4, the latter embodying the recovery phase of the PETM (Pujalte et al. 2014).

The hypotheses that channel-body amalgamation at the PETM resulted from either subsidence reduction or relative sea-level fall can be discarded on the basis of knowledge of the inferred

582 regime of tectonic quiescence and relative sea-level rise at the Paleocene-Eocene boundary
583 (Pujalte et al. 2014).
584 Schmitz & Pujalte (2007) interpreted the increase in channel-body density seen in the member 2
585 (Claret Conglomerate) as representing the progradation of a braidplain that formed the proximal
586 portion of a megafan. However, this geomorphic interpretation contrasts with converging
587 palaeoflow directions away from the catchments (cf. Pujalte et al. 2014), and no data are available
588 to indicate that the Claret Conglomerate represents a suite of deposits associated with a single fan,
589 rather than with coalescing landforms. A scenario invoking a single megafan appears unlikely in
590 consideration of the complex topography on which the member 2 accumulated, as expressed in
591 the geometry and lateral discontinuity of the member 1. Given that these valley fills are believed to
592 record a single phase of incision and infill (Pujalte et al. 2014), and in consideration of the limited
593 distance between the catchments and the palaeoshoreline, the presence of multiple valley fills
594 suggests the persistence of multiple entry points in the neighbouring mountain front during phases
595 of widespread aggradation; the spacing of these valley fills might reflect the spacing of long-lived
596 feeder valleys . Additionally, the deposits of the Claret Conglomerate are locally interpretable as
597 the product of accumulation of gravelly channel lags, in relation to which overlying sand-prone
598 deposits of the member 3 – which is largely established on pedogenic characteristics – are
599 genetically related and synchronous (cf. figure 6E). Thus, the Claret Conglomerate alone, as a
600 lithostratigraphic unit, cannot be interpreted in palaeogeomorphic terms.
601
602 Controls on environmental change
603 Intervals that encompass the PETM are also characterized by channel complexes that are, on
604 average, slightly thicker than channel complexes from pre-PETM units. This observation likely
605 reflects the increased degree of channel-body amalgamation, which is also expressed by a higher
606 proportion of multi-storey and multi-lateral channel complexes in the syn-PETM member 2 of the
607 Claret Formation, as compared to the pre-PETM member 1.

608 The thickness of channel fills and barforms is relatively uniform across the studied stratigraphy,
609 which can be interpreted in terms of largely unchanged maximum bankfull depth of formative fluvial
610 channels. If the existence of rivers with comparable size and channel-forming discharges across
611 the PETM is assumed, the observed channel-body amalgamation could then be explained by
612 enhanced channel mobility through faster lateral migration or more frequent avulsion (Bristow &
613 Best 1993). However, it must be considered that the exhibited characters may also emerge in
614 relation to the development of a network of roughly equally sized channels that form a multi-thread
615 wandering or braided river, as opposed to a single-thread fluvial system. A braided river could
616 accommodate a larger total water discharge and would be characterized by wider channel belts,
617 the latter character being typically incorporated in the rock record in the form of wider channel
618 complexes, by comparison with single-thread counterparts (cf. Schumm 1985; Gibling 2006;
619 Colombera et al. 2013).
620 The hypothesis that channel-body amalgamation at the PETM resulted from increased channel
621 mobility can be related to two fundamentally different categories of environmental change, which
622 are not mutually exclusive:
623 1) changes in the drainage catchments that would drive an increase in channel mobility in the
624 basin; such a change in river behaviour might have been caused by greater bedload delivery or
625 reduced fine-grained suspended load delivery, which could have resulted in higher channel erosive
626 power (cf. Nanson & Hickin 1986), faster in-channel deposition (cf. Howard 1992; Wickert et al.
627 2013), and perhaps decreased bank stability resulting from changes in stream-bank texture (e.g.,
628 reduced clay content; cf. Thorne 1991); increased water discharge or discharge variability could
629 also have played a role by increasing transport flux and avulsion frequency (cf. Howard 1992;
630 Jones & Schumm 1999).
631 2) changes in the nature of the depositional basin, which would permit the channels to be
632 more mobile in relation to increased bank erodibility, for example through variations in vegetation
633 type and density (cf. Gyssels et al. 2005), in organic-matter content (controlling soil aggregation;

634 Morgan 2005), or in soil drainage (positive pore water pressures reduce the effective cohesion of a
635 soil; Thorne 1991).
636 Although the average thickness of barforms and channel fills shows limited change across the
637 stratigraphy, a significant increase in thickness variability is seen across the members 1 and 2/3,
638 which could signify more variable channel-forming water discharge during the PETM interval.
639 Again, in view of the multi-storey and multi-lateral character of many channel complexes in the
640 members 2 and 3, this may be related to the development of a network of variably sized channels
641 within the braidplain setting envisaged by Schmitz & Pujalte (2007) and Dreyer (1993).
642 Indicative values of mean dune height and formative flow depth can be derived from cross-set
643 thickness distributions of cross-stratified sandstones using existing empirical relationships (Allen
644 1970; Bridge & Tye 2000; Leclair & Bridge 2001): this approach returns estimated mean bankfull
645 depths of 4.0 m for the Esplugafreda Formation, 3.6 m for the member 1, and 5.2 m for the
646 members 2/3. However, the coefficient of variation of cross-set thickness suggests that the
647 empirical relationships used are unreliable in application to the Claret Formation dataset (cf. Bridge
648 & Tye 2000), and hence results, which would suggest increased bankfull depth during the PETM,
649 are uncertain.
650 A significant change in the facies organization of channel deposits is recorded across the transition
651 between the Esplugafreda and Claret formations. The facies associations and sedimentary
652 characteristics of the Esplugafreda Formation channel bodies have been interpreted to be typical
653 of a system subject to an ephemeral discharge regime (Dreyer 1993): the Esplugafreda Formation
654 channel complexes are characterized by pause planes, a dominantly aggradational channel-fill
655 style connected with lack of evident barform development, and a relatively high proportion of plane-
656 bedded or low-angle cross-stratified sandstones (Sh, Sl), which can be related to transcritical to
657 supercritical flow conditions (Fielding 2006). A shift from ephemeral to more perennial conditions
658 may be recorded at the transition between the Esplugafreda and Claret formations (cf. Dreyer
659 1993), as evidenced by decreased frequency of pause planes (which appear to be absent from

660 member 2), enhanced bar-form development, increase in the presence of structures relating to
661 two- and three-dimensional dunes, and observation of cross-set thickness of sandy units being
662 less variable and on average thicker – which may reflect dune height increase from the upper-
663 stage plane bed to the dune stability field (Leclair & Bridge 2001). However, proportions of facies-
664 unit types within the Claret Formation appear to vary little when the member 1 and the members 2
665 and 3 are compared: this suggests that the most significant change in channel-filling processes
666 may have predated the onset of the PETM, and that the Garumnian system evolved relatively little
667 in terms of in-channel depositional processes at the PETM compared to its immediate past. Based
668 on inferences regarding the span of time embodied by the member 1 valley fills (i.e., in the order of
669 10^4 yr; Pujalte et al. 2014), the change in fluvial-channel facies observed across the Esplugafreda
670 Formation and the member 1, and the concurrent change in palaeosol characteristics, might
671 represent a response to the warming trend that is thought to have immediately preceded the
672 carbon release recorded in the CIE (Secord et al. 2010; cf. Bowen et al. 2015).
673 Also, in contrast to what is stated by Schmitz & Pujalte (2007), no dramatic change is observed in
674 the distribution of maximum extraclast size in channel fills and barforms across the Claret
675 Formation members 2 and 3, relative to the pre-PETM member 1, suggesting that the Garumnian
676 streams in the Arén area did not undergo any major variation in flow competence through the
677 Paleocene-Eocene boundary. This is not entirely unexpected given that the member 1 channel
678 complexes sit inside base-level-controlled incised-valley fills (Pujalte et al. 2014), and were
679 therefore probably associated with a higher gradient than the member 2 and 3 channel complexes.
680 Thus, the most evident architectural change across the PETM is in the degree of channel-body
681 amalgamation, which can be related to both intra- and extra-basinal factors on formative-channel
682 network characteristics (number of active channels, channel pattern) and mobility (in relation to
683 channel and bank characteristics).
684 Variations in sediment supply calibre and rate may be associated with climate-driven changes in
685 weathering mechanisms, rates and erodibility. A scenario of transient PETM wetting seems in

686 accord with the presence of grey low-chroma deposits with coaly fragments in parts of the member
687 2 of the Claret Formation, transitional upwards to the yellowish palaeosol of member 3, and
688 possibly representing the product of gleying related to waterlogged conditions connected to a
689 water-table rise of climatic origin; however, the first occurrence of grey palaeosols in the study
690 interval is recognized in the valley fills of the member 1. Intensified land erosion related to both
691 seasonal extreme precipitation and sparser vegetation cover was postulated by Schmitz & Pujalte
692 (2003; cf. Schmitz et al. 2001), in part on the basis of increased accumulation rates of terrigenous
693 detritus in marine strata that are correlative to the members 2 and 3. It is significant that, whereas
694 member 1 of the Claret Formation comprises deposits that onlap the palaeotopography that marks
695 the base of member 1 itself, the same palaeotopography appears instead to be sharply truncated
696 by the base of member 2, as evident near the palaeovalley margins and expressed in the
697 horizontal continuity of the Claret Conglomerate (figure 6E). The relationship between the
698 interfluves of the pre-PETM valleys and the PETM deposits, and in particular the geometry of the
699 contact, have been previously described (Baceta et al. 2011; Pujalte et al. 2014), but its
700 significance has been in part overlooked. The planation of the interfluves can be inferred to have
701 occurred immediately prior to, or penecontemporaneously with, accumulation of member 2 (figure
702 13); this suggests either an increase in the erodibility of the interfluves, or in the erosive power of
703 the Garumnian streams, at the onset of the PETM. The rapid erosional demolition of the interfluves
704 would account for the increase in the rate of supply of fine-grained terrigenous sediment and
705 progradation of clastic facies belts that are inferred to have occurred basinwide (Pujalte et al. 2015;
706 2016). The availability of sediment from neighbouring interfluves, together with the proximity of the
707 drainage areas, might have resulted in a limited lag time between PETM onset and response of the
708 river system in the Arén sector (cf. Manners et al. 2013; 2014; Pujalte & Schmitz 2014). Greater
709 delivery of coarse-grained sediment to the Garumnian streams during the PETM may have
710 enhanced channel erosive power and flow splitting and accelerated in-channel deposition, thereby
711 increasing channel instability. However, it is unclear whether increased river mobility drove an

712 increase in sediment supply by eroding interfluve areas, or rather the increased sediment yield
713 determined faster river mobility that in turned favoured interfluve erosion. Additionally, the onset of
714 seasonality in water discharge advocated by Schmitz & Pujalte (2003) could also be considered in
715 relation to its control on avulsion frequency (cf. Jones & Schumm 1999; Leier et al. 2005; Plink-
716 Björklund 2015). However, sedimentological evidence indicates that if a more peaked discharge
717 regime characterized by high-magnitude events existed for the PETM, this left no distinctive
718 signature in the lithofacies of channel deposits (e.g., in the form of variations in proportions of
719 sedimentary structures that may represent the record of conditions transitional to or within the
720 upper flow-regime, thought to be frequent under seasonal climates; cf. Fielding 2006; Fielding et al.
721 2009; Plink-Björklund 2015), and was likely established on a background of more perennial base
722 discharge for the Claret Formation rivers as compared to rivers of the Esplugafreda Formation.
723

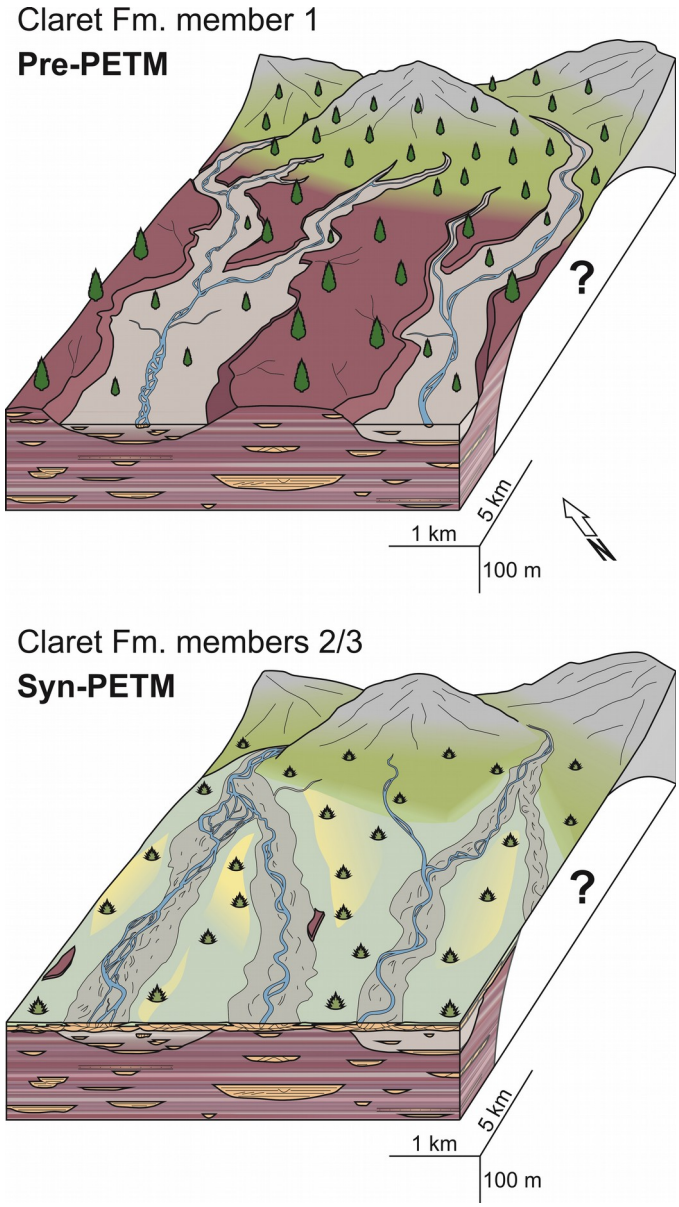

Figure 13: block diagrams that illustrate the interpreted palaeogeography for the pre- and syn-PETM intervals of the Claret Formation in the Arén area, and how the geomorphic evolution of the system across the PETM is now expressed in the stratigraphic architecture of the succession. Note the rapid transition from a stage of valley backfilling to erosional demolition of valley interfluves and widespread aggradation.

In terms of intra-basinal controls, a reduction in stream-bank stability may have resulted in response to positive pore water pressures, which reduce soil effective cohesion, or to sparser

732 riparian vegetation. Inferences of increased channel instability and change in dominant planform
733 morphology for the Garumnian streams at the PETM is compatible with the vegetation changeover
734 indicated by the palynological record of the Basque Basin catchments, and consisting in the
735 inferred replacement of permanent conifer forests with a seasonal cover (Schmitz et al. 2001).
736
737 Comparison with other fluvial systems
738 Other continental successions that contain a record of the PETM and of the response of mid-
739 latitude river systems to the event are recognized in the Piceance and Bighorn basins, USA (Koch
740 et al. 1995; Bowen et al. 2001; Burger 2012; Foreman et al. 2012). Although a detailed analysis is
741 beyond the scope of this work, detecting commonalities between these depositional systems is
742 useful for assessing whether variations in sedimentary architecture observed through the PETM in
743 the Tremp-Graus Basin might reflect global or local environmental change. It is particularly
744 significant that increased channel-body density is also seen in both the Piceance and Bighorn
745 basins in intervals that correspond to or contain the PETM, and that lag times in the responses are
746 similarly identified, albeit of variable duration (Foreman et al. 2012; Foreman 2014). Recognition of
747 this particular stratigraphic signature in the different basins may reflect similar responses of fluvial
748 landscapes and associated geomorphic processes to analogous climate-driven environmental
749 change. Whereas a similar evolution is seen in terms of channel-body density and geometries in
750 the Tremp-Graus, Piceance and Bighorn basins, data on facies organization (grainsize,
751 sedimentary structures) indicate that the response of channel-filling processes to the PETM was
752 variable in terms of both magnitude of change and type of depositional processes involved (cf.
753 Foreman et al. 2012; Foreman 2014). This fact suggests that if a common control determined the
754 emergence of similar large-scale stratigraphic trends, this should be a factor that dominates in
755 controlling river mobility and size, but may be overridden by other processes in controlling
756 depositional mechanisms. Given the current knowledge of basin histories, as constrained by
757 available proxies on tectonic, climatic, and sea-level controls, a number of potential factors may

758 have plausibly determined an increase in the mobility, number and/or size of fluvial channels at the
759 PETM across all these systems: hydrological change, increased clastic influx, and variations in
760 type and density of vegetation cover – which are themselves partially inter-related.
761
762 **Conclusions**
763 A quantitative sedimentological analysis has been carried out on outcrops of sedimentary deposits
764 of the Tremp-Graus Basin to assess the geomorphic response of an alluvial system to environ-
765 mental change through the PETM. Outcrops in the Arén area offer insight into the geomorphic
766 change of a fluvial landscape characterized by a complex topography before the PETM. As previ-
767 ously recognized, the onset of the PETM marks a transition between a phase of deposition within
768 the confines of a valley network to a phase of widespread aggradation; this transition is here inter-
769 preted to be caused by the rapid destruction of valley interfluves by syn-PETM streams, rather than
770 by complete valley backfilling. This inference is compatible with scenarios of increased substrate
771 erodibility or increased erosive power of the streams, at the PETM, and will likely have resulted in,
772 and might in part have been determined by, higher rates of sediment supply. Whereas the propor-
773 tion, thickness and width of fluvial channel complexes is seen to increase through the PETM strati-
774 graphy, the thickness and maximum grain size of channel fills and barforms does not change signi-
775 ficantly, suggesting limited variations in maximum bankfull depth and competence of fluvial chan-
776 nels, and indicating that the observed channel-body amalgamation might be due to higher rates of
777 lateral migration, higher avulsion frequency, or development of a braided network. Recognition of
778 this particular stratigraphic signature may reflect a response of the fluvial landscape and processes
779 to types of climate-driven environmental change in accordance with what has previously been sug-
780 gested for this basin, i.e., in relation to enhanced hydrological cycle, increased seasonality, and ve-
781 getation loss. However, the facies organization of syn-PETM channel deposits of the Claret Forma-
782 tion does not appear to be significantly different from that seen in the immediately preceding pre-
783 PETM channel bodies of member 1.

Because the analysed characteristics of fluvial sedimentary architecture represent a record of river processes and landforms, the studied succession might represent an analogue with which to predict the geomorphic metamorphosis of river systems in certain mid-latitude regions under conditions of rapid global warming. However, further research on the Tremp Group is required to better constrain the relative importance of specific factors and to elucidate the behaviour of the river network at the scale of the entire basin.

Acknowledgements

The FRG-ERG sponsors (Areva, BHP Billiton, ConocoPhillips, Aker BP, Murphy Oil Corporation, Nexen, Petrotechnical Data Systems, Saudi Aramco, Shell, Tullow Oil, Woodside, and YPF) are thanked for their financial support. LC has been supported by NERC (Catalyst Fund award NE/M007324/1; Follow-on Fund NE/N017218/1). Marco Patacci is thanked for his help in the field. We thank Piret Plink-Björklund and Nicola Minelli for commenting an earlier version of part of this manuscript. Two anonymous reviewers are thanked for constructive comments that improved the article.

References

Adatte, T., Khozyem, H., Spangenberg, J. E., Samant, B., & Keller, G. (2014). Response of terrestrial environment to the Paleocene-Eocene Thermal Maximum (PETM), new insights from India and NE Spain. In: Dickens, G. R., & Luciani, V. (eds.) Climatic and biotic events of the Paleogene 2014, Rendiconti Online della Società Geologica Italiana, 31, 5-6.

Allen, J. R. L. (1970) Physical processes of sedimentation. London Allen and Unwin, 248 pp.

Arostegi, J., Baceta, J. I., Pujalte, V., & Carracedo, M. (2011). Late Cretaceous–Palaeocene mid-latitude climates: inferences from clay mineralogy of continental-coastal sequences (Tremp-Graus area, southern Pyrenees, N Spain). Clay Minerals, 46, 105-126.

Baceta, J. I., Pujalte, V., Wright, V. P., & Schmitz, B. (2011). Carbonate platform models, sea-level changes and extreme climatic events during the Paleocene/early Eocene greenhouse interval. In: Arenas, C., Pomar, L., & Colombo F. (eds.) Pre-Meeting field-trips guidebook, 28th IAS Meeting, Zaragoza. Sociedad Geológica de España, Geo-Guías, 7, 101-150.

Barrón, E., Rivas-Carballo, R., Postigo-Mijarra, J. M., Alcalde-Olivares, C., Vieira, M., Castro, L., Pais, J., & Valle-Hernández, M. (2010). The Cenozoic vegetation of the Iberian Peninsula: a synthesis. Review of Palaeobotany and Palynology, 162, 382-402.

Berástegui, X., García-Senz, J., & Losantos, M. (1990). Tectono-sedimentary evolution of the Organyà extensional basin (central south Pyrenean unit, Spain) during the Lower Cretaceous. Bulletin de la Société Géologique de France, 6, 251-264.

Bhattacharya, J. P., & Tye, R. S. (2004). Searching for modern Ferron analogs and application to subsurface interpretation. In: Chidsey, T. C. Jr, Adams, R. D., & Morris, T. H. (eds.) Regional to wellbore analog for fluvial-deltaic reservoir modeling: The Ferron Sandstone of Utah, AAPG Studies in Geology, 50, 39-57.

Bolle, M. P., & Adatte, T. (2001). Palaeocene-early Eocene climatic evolution in the Tethyan realm: clay mineral evidence. Clay Minerals, 36, 249-261.

Bond, R. M. G., & McClay, K. R. (1995). Inversion of a Lower Cretaceous extensional basin, south central Pyrenees, Spain. In: Buchanan, J. G., & Buchanan, P. G. (eds.) Basin inversion, Geological Society, London, Special Publications, 88, 415-431.

Bonett, D. G. (2006). Robust confidence interval for a ratio of standard deviations. Applied Psychological Measurements, 30, 432-439.

Bowen, G. J., Koch, P. L., Gingerich, P. D., Norris, R. D., Bains, S., & Corfield, R. M. (2001). Refined isotope stratigraphy across the continental Paleocene-Eocene boundary on Polecat Bench in the northern Bighorn Basin. In: Gingerich, P. D. (ed.) Paleocene-Eocene stratigraphy and biotic change in the Bighorn and Clarks Fork basins, Wyoming. University of Michigan Papers on Paleontology, 33, 73-88.

Bowen, G. J., Maibauer, B. J., Kraus, M. J., Röhl, U., Westerhold, T., Steimke, A., Gingerich, P. D., Wing, S. L., & Clyde, W. C. (2015). Two massive, rapid releases of carbon during the onset of the Palaeocene-Eocene thermal maximum. Nature Geoscience, 8, 44-47

Bridge, J. S. (2003). Rivers and Floodplains. Blackwell, Oxford, 491 pp.

Bridge, J. S., & Tye, R. S. (2000). Interpreting the dimensions of ancient fluvial channel bars, channels, and channel belts from wireline-logs and cores. AAPG Bulletin, 84, 1205-1228.

Bristow, C.S., & Best, J.L. (1993). Braided rivers: Perspectives and problems. In: Best, J.L., & Bristow, C.S. (eds.) Braided Rivers, Geological Society, London, Special Publication, 75, 1-11.

Burbank, D. W., Vergés, J., Munoz, J. A., & Bentham, P. (1992). Coeval hindward-and forward-imbricating thrusting in the south-central Pyrenees, Spain: Timing and rates of shortening and deposition. Geological Society of America Bulletin, 104, 3-17.

Burger, B. J. (2012). Northward range extension of a diminutive-sized mammal (Ectocion parvus) and the implication of body size change during the Paleocene–Eocene Thermal Maximum. Palaeogeography, Palaeoclimatology, Palaeoecology, 363, 144-150.

Butterlin, J., Vrielynck, B., Bignot, G., Clermonte, J., Colchen, M., Dercourt, J., Guiraud, R., Poisson, A., & Ricou, L. E. (1993). Lutetian (46–40 Ma). In: Dercourt, J., Ricou, L. E., & Vrielynck, B. (eds.) Atlas of Tethys paleoenvironmental maps. Gauthiers Villars, Paris, 197-209.

Charles, A. J., Condon, D. J., Harding, I. C., Pälike, H., Marshall, J. E., Cui, Y., Kump, L., & Croudace, I. W. (2011). Constraints on the numerical age of the Paleocene/Eocene boundary. Geochemistry, Geophysics, Geosystems, 12, Q0AA17.

Colombera, L., Mountney, N. P., & McCaffrey, W. D. (2012). A relational database for the digitization of fluvial architecture concepts and example applications. Petroleum Geoscience, 18, 129-140.

Colombera, L., Mountney, N. P., & McCaffrey, W. D. (2013). A quantitative approach to fluvial facies models: Methods and example results. Sedimentology, 60, 1526-1558.

Cuevas, J. L. (1992). Estratigrafía del" Garumniense" de la Conca de Tremp. Prepirineo de Lérida. Acta Geológica Hispánica, 27, 95-108.

886 Dallanave, E., Tauxe, L., Muttoni, G., & Rio, D. (2010). Silicate weathering machine at work: rock
887 magnetic data from the late Paleocene–early Eocene Cicogna section, Italy. Geochemistry,
888 Geophysics, Geosystems, 11(7), Q07008.
889
890 Dawson, A., Grimes, S., Ellis, M., Duller, R., Watkinson, M., Stokes, M., & Leng, M. J. (2014). Initial
891 paleohydrological observations from the Paleocene-Eocene boundary at Esplugafreda and
892 Berganuy in northern Spain. In: Dickens, G. R., & Luciani, V. (eds.) Climatic and biotic events of
893 the Paleogene 2014, Rendiconti Online della Società Geologica Italiana, 31, 54-55.
894
895 Domingo, L., López-Martínez, N., Leng, M. J., & Grimes, S. T. (2009). The Paleocene–Eocene
896 Thermal Maximum record in the organic matter of the Claret and Tendruy continental sections
897 (South-central Pyrenees, Lleida, Spain). Earth and Planetary Science Letters, 281(3), 226-237.
898
899 Dreyer, T. (1993). Quantified fluvial architecture in ephemeral stream deposits of the Esplugafreda
900 Formation (Palaeocene), Tremp-Graus Basin, northern Spain. In: Marzo, M., & Puigdefábregas, C.
901 (eds.) Alluvial sedimentation: International Association of Sedimentologists Special Publication, 17,
902 337-362.
903
904 Dypvik, H., Riber, L., Burca, F., Rüther, D., Jargvoll, D., Nagy, J., & Jochmann, M. (2011). The
905 Paleocene–Eocene thermal maximum (PETM) in Svalbard – clay mineral and geochemical
906 signals. Palaeogeography, Palaeoclimatology, Palaeoecology, 302, 156-169.
907
908 Eichenseer, H., & Luterbacher, H. (1992). The marine Paleogene of the Tremp Region (NE Spain)-
909 depositional sequences, facies history, biostratigraphy and controlling factors. Facies, 27, 119-151.
910

911 Farrell, S. G., Williams, G. D., & Atkinson, C. D. (1987). Constraints on the age of movement of the
912 Montsech and Cotiella Thrusts, south central Pyrenees, Spain. Journal of the Geological Society,
913 144, 907-914.
914
915 Feist, M., & Colombo, F. (1983) La limite Crétacé-Tertiaire dans le nord-est de l'Espagne, du point
916 de vue des charophytes. Géologie Méditerranéenne, 10, 303-326.
917
918 Fernández, O., Muñoz, J. A., Arbués, P., & Falivene, O. (2012). 3D structure and evolution of an
919 oblique system of relaying folds: the Ainsa basin (Spanish Pyrenees). Journal of the Geological
920 Society, 169, 545-559.
921
922 Fielding, C. R. (2006). Upper flow regime sheets, lenses and scour fills: extending the range of
923 architectural elements for fluvial sediment bodies. Sedimentary Geology, 190, 227-240.
924
925 Fielding, C. R., Allen, J. P., Alexander, J., & Gibling, M. R. (2009). Facies model for fluvial systems
926 in the seasonal tropics and subtropics. Geology, 37, 623-626.
927
928 Filleaudeau, P. Y., Mouthereau, F., & Pik, R. (2012). Thermo-tectonic evolution of the south-central
929 Pyrenees from rifting to orogeny: insights from detrital zircon U/Pb and (U-Th)/He
930 thermochronometry. Basin Research, 24, 401-417.
931
932 Foreman, B. Z. (2014). Climate-driven generation of a fluvial sheet sand body at the Paleocene-
933 Eocene boundary in north-west Wyoming (USA). Basin Research, 26, 225-241.
934
935 Foreman, B. Z., Heller, P. L., & Clementz, M. T. (2012). Fluvial response to abrupt global warming
936 at the Palaeocene/Eocene boundary. Nature, 491, 92-95.

García Veigas, J. (1997). First continental evaporitic phase in the South Pyrenean Central area: Tremp Gypsum (Garumn Facies, Upper Paleocene; Allochtonous Zone). In: Busson, G., & Schreiber, B. C. (eds.) Sedimentary deposition in rift and foreland basins in France and Spain (Paleogene and Lower Neogene). Columbia University Press, 335-342.

Gibling, M. R. (2006). Width and thickness of fluvial channel bodies and valley fills in the geological record: a literature compilation and classification. Journal of Sedimentary Research, 76, 731-770.

Gómez-Gras, D., Roigé, M., Fondevilla, V., Oms, O., Boya, S., & Remacha, E. (2016). Provenance constraints on the Tremp Formation paleogeography (southern Pyrenees): Ebro Massif *VS* Pyrenees sources. Cretaceous Research, 57, 414-427.

Gyssels, G., Poesen, J., Bochet, E., & Li, Y. (2005). Impact of plant roots on the resistance of soils to erosion by water: a review. Progress in Physical Geography, 29, 189-217.

Hajek, E. A., & Heller, P. L. (2012). Flow-depth scaling in alluvial architecture and nonmarine sequence stratigraphy: example from the Castlegate Sandstone, Central Utah, USA. Journal of Sedimentary Research, 82, 121-130.

Howard, A. D. (1992). Modeling channel migration and floodplain sedimentation in meandering streams. In: Carling, P. A., & Petts, G. E. (eds.) Lowland floodplain rivers: Geomorphological perspectives, 1-41.

961 Jones, L. S., & Schumm, S. A. (1999). Causes of avulsion: an overview. In: Smith, N.D., & Rogers,
962 J. (eds.) Fluvial Sedimentology VI. Special Publication of the International Association of Sedi-
963 mentologists, 28, 171-178.
964
965 Kennett, J. P., Stott, L. D. (1991). Abrupt deep-sea warming, palaeoceanographic changes and
966 benthic extinctions at the end of the Paleocene. Nature, 353, 225-229.
967
968 Koch, P. L., Zachos, J. C., & Gingerich, P. D. (1992). Correlation between isotope records in mar-
969 ine and continental carbon reservoirs near the Palaeocene/Eocene boundary. Nature, 358, 319-
970 322.
971
972 Koch, P. L., Zachos, J. C., & Dettman, D. L. (1995). Stable isotope stratigraphy and paleoclimato-
973 logy of the Paleogene Bighorn Basin (Wyoming, USA). Palaeogeography, Palaeoclimatology, Pa-
974 laeoecology, 115, 61-89.
975
976 Kraus, M. J., Woody, D. T., Smith, J. J., & Dukic, V. (2015). Alluvial response to the Paleocene–Eo-
977 cene Thermal Maximum climatic event, Polecat Bench, Wyoming (USA). Palaeogeography, Pa-
978 laeoclimatology, Palaeoecology, 435, 177-192.
979
980 Latrubesse, E. M. (2015). Large rivers, megafans and other Quaternary avulsive fluvial systems: A
981 potential “who's who” in the geological record. Earth-Science Reviews, 146, 1-30.
982
983 Leclair, S. F., & Bridge, J. S. (2001). Quantitative interpretation of sedimentary structures formed by
984 river dunes. Journal of Sedimentary Research, 71, 713-716.
985

Leier, A. L., DeCelles, P. G., & Pelletier, J. D. (2005). Mountains, monsoons, and megafans. Geology, 33, 289-292.

López-Martínez, N., & Peláez-Campomanes, P. (1999). New mammals from south-central Pyrenees (Tremp Formation, Spain) and their bearing on late Paleocene marine-continental correlations. Bulletin de la Société Géologique de France, 170, 681-696.

López-Martínez, N., Dinarés-Turell, J., & Elez, J. (2006). Chronostratigraphy of the continental Paleocene series from the South Central Pyrenees (Spain): new magnetostratigraphic constraints. In: Caballero, F., Apellaniz, E., Baceta, J.I., Bernaola, G., Orue-Etxebarria, X., Payros, A., Pujalte, V. (eds.) Climate and Biota of the Early Paleogene, Bilbao 2006, Volume of Abstracts, 83.

Lunt, I. A., Smith, G. H. S., Best, J. L., Ashworth, P. J., Lane, S. N., & Simpson, C. J. (2013). Deposits of the sandy braided South Saskatchewan River: Implications for the use of modern analogs in reconstructing channel dimensions in reservoir characterization. AAPG Bulletin, 97, 553-576.

Luterbacher, H. (1998). Sequence Stratigraphy and the Limitations of Biostratigraphy in the Marine Paleogene Strata of the Tremp Basin (Central Part of the Southern Pyrenean Foreland Basins, Spain). In: De Graciansky, P. C., Hardenbol, J., Jacquin T., & Vail, P. R. (eds.) Mesozoic and Cenozoic sequence stratigraphy of European basins. SEPM Special Publication, 60, 303-309.

Luterbacher, H. P., Eichenseer, H., Betzler, C., & Van den Hurk, A. M. (1991). Carbonate-siliciclastic depositional systems in the Paleogene of the South Pyrenean foreland basin: a sequence-stratigraphic approach. In: Macdonald, D. I. M. (ed.) Sedimentation, Tectonics and Eustasy: Sea-Level Changes at Active Margins. Special Publication of the International Association of Sedimentologists, 12, 391-407.

Manners, H. R., Grimes, S. T., Sutton, P. A., Domingo, L., Leng, M. J., Twitchett, R. J., Hart, M. B., Dunkley Jones, T., Pancost, R. D., Duller, R., & Lopez-Martinez, N. (2013). Magnitude and profile of organic carbon isotope records from the Paleocene–Eocene Thermal Maximum: Evidence from northern Spain. Earth and Planetary Science Letters, 376, 220-230.

Manners, H. R., Grimes, S. T., Sutton, P. A., Domingo, L., Leng, M. J., Twitchett, R. J., Hart, M. B., Dunkley Jones, T., Pancost, R. D., Duller, R., & Lopez-Martinez, N. (2014). Reply to comment on "Magnitude and profile of organic carbon isotope records from the Paleocene–Eocene Thermal Maximum: Evidence from northern Spain" by Manners et al. [Earth Planet. Sci. Lett. 376 (2013) 220–230]. Earth and Planetary Science Letters, 395, 294-295.

McInerney, F. A., & Wing, S. L. (2011). The Paleocene-Eocene thermal maximum: a perturbation of carbon cycle, climate, and biosphere with implications for the future. Annual Review of Earth and Planetary Sciences, 39, 489-516.

Médus, J., & Colombo, F. (1991) Succession climatique et limite stratigraphique Crétacé-Tertiaire dans le N.E. de l'Espagne. Acta Geológica Hispánica, 26, 173-179.

Miall, A. D. (1996). The geology of fluvial deposits: sedimentary facies, basin analysis, and petroleum geology. Springer Verlag, Berlin, 582 pp.

Miall, A. D., & Jones, B. G. (2003). Fluvial architecture of the Hawkesbury sandstone (Triassic), near Sydney, Australia. Journal of Sedimentary Research, 73, 531-545.

1037 Miller, K. G., Kominz, M. A., Browning, J. V., Wright, J. D., Mountain, G. S., Katz, M. E., Sugarman,
1038 P. J., Cramer, B. S., Christie-Blick, N., & Pekar, S. F. (2005). The Phanerozoic record of global
1039 sea-level change. Science, 310, 1293-1298.
1040
1041 Minelli, N., Manzi, V., & Roveri, M. (2013). The record of the Paleocene-Eocene thermal maximum
1042 in the Ager Basin (Central Pyrenees, Spain). Geologica Acta, 11, 421-441.
1043
1044 Mohrig, D., Heller, P. L., Paola, C., & Lyons, W. J. (2000). Interpreting avulsion process from an-
1045 cient alluvial sequences: Guadalope-Matarranya system (northern Spain) and Wasatch Formation
1046 (western Colorado). Geological Society of America Bulletin, 112, 1787-1803.
1047
1048 Morgan, R. P. C. (2005). Soil erosion and conservation. John Wiley & Sons. 304 pp.
1049
1050 Mutti, E., Davoli, G., Tinterri, R., & Zavala, C. (1996). The importance of ancient fluvio-deltaic sys-
1051 tems dominated by catastrophic flooding in tectonically active basins. Memorie di Scienze
1052 Geologiche, 48, 233-291.
1053
1054 Mutti, E., Tinterri, R., Di Biase, D., Fava, L., Mavilla, N., Angella, S., & Calabrese, L. (2000). Delta-
1055 front facies associations of ancient flood-dominated fluvio-deltaic systems. Revista de la Sociedad
1056 Geológica de España, 13, 165-190.
1057
1058 Nanson, G. C., & Hickin, E. J. (1986). A statistical analysis of bank erosion and channel migration
1059 in western Canada. Geological Society of America Bulletin, 97, 497-504.
1060
1061 Ori, G. G., & Friend, P. F. (1984). Sedimentary basins formed and carried piggyback on active
1062 thrust sheets. Geology, 12, 475-478.

Payros, A., Pujalte, V., Baceta, J. I., Bernaola, G., Orue-Etxebarria, X., Apellaniz, E., Caballero, F. & Ferrnadez, C. (2000). Lithostratigraphy and sequence stratigraphy of the upper Thanetian to middle llerdian strata of the Campo section (southern Pyrenees, Spain): Revision and new data. Revista de la Sociedad Geológica de España, 13, 213-226.

Plaziat, J. C. (1981). Late Cretaceous to Late Eocene palaeogeographic evolution of southwest Europe. Palaeogeography, Palaeoclimatology, Palaeoecology, 36, 263-320.

Plink-Björklund, P. (2015). Morphodynamics of rivers strongly affected by monsoon precipitation: Review of depositional style and forcing factors. Sedimentary Geology, 323, 110-147.

Puigdefàbregas, C., & Souquet, P. (1986). Tecto-sedimentary cycles and depositional sequences of the Mesozoic and Tertiary from the Pyrenees. Tectonophysics, 129, 173-203.

Puigdefàbregas, C., Muñoz, J. A., & Vergés, J. (1992). Thrusting and foreland basin evolution in the southern Pyrenees. In: McClay, K. R. (ed.) Thrust tectonics, Springer Netherlands, 247-254.

Pujalte, V., & Schmitz, B. (2005). Revisión de la estratigrafía del Grupo Tremp («Garumniense», Cuenca de Tremp-Graus, Pirineos meridionales). Geogaceta, 38,
79-82.

Pujalte, V., & Schmitz, B. (2014). Comment on “Magnitude and profile of organic carbon isotope records from the Paleocene–Eocene Thermal Maximum: Evidence from northern Spain” by Manners et al. [Earth Planet. Sci. Lett. 376 (2013) 220–230]. Earth and Planetary Science Letters, 395, 291-293.

Pujalte, V., Schmitz, B., Baceta, J. L., Orue-Etxebarria, X., Bernaola, G., Dinarés-Turell, J., Payros, A., Apellaniz, E., & Caballero, F. (2009). Correlation of the Thanetian-Ilerdian turnover of larger foraminifera and the Paleocene-Eocene thermal maximum: confirming evidence from the Campo area (Pyrenees, Spain). Geologica Acta, 7, 161-175.

Pujalte, V., Schmitz, B., & Baceta, J. I. (2014). Sea-level changes across the Paleocene–Eocene interval in the Spanish Pyrenees, and their possible relationship with North Atlantic magmatism. Palaeogeography, Palaeoclimatology, Palaeoecology, 393, 45-60.

Pujalte, V., Baceta, J. I., & Schmitz, B. (2015). A massive input of coarse-grained siliciclastics in the Pyrenean Basin during the PETM: the missing ingredient in a coeval abrupt change in hydrological regime. Climate of the Past, 11, 1653-1672.

Pujalte, V., Robador, A., Payros, A., & Samsó, J. M. (2016). A siliciclastic braid delta within a lower Paleogene carbonate platform (Ordesa-Monte Perdido National Park, southern Pyrenees, Spain): record of the Paleocene–Eocene thermal maximum perturbation. Palaeogeography, Palaeoclimatology, Palaeoecology, 459, 453-470.

Rasser, M. W., Scheibner, C., & Mutti, M. (2005). A paleoenvironmental standard section for Early Ilerdian tropical carbonate factories (Corbieres, France; Pyrenees, Spain). Facies, 51, 218-232.

Rosell, J., Linares, R., & Llompart, C. (2001). El “Garumniense” prepirenaico. Revista de la Sociedad Geológica de España, 14, 47-56.

1114 Schmitz, B., & Pujalte, V. (2003). Sea-level, humidity, and land-erosion records across the initial
1115 Eocene thermal maximum from a continental-marine transect in northern Spain. Geology, 31, 689-
1116 692.
1117
1118 Schmitz, B., & Pujalte, V. (2007). Abrupt increase in seasonal extreme precipitation at the Paleo-
1119 cene-Eocene boundary. Geology, 35, 215-218.
1120
1121 Schmitz, B., Pujalte, V., & Nunez-Betelu, K. (2001). Climate and sea-level perturbations during the
1122 Incipient Eocene Thermal Maximum: evidence from siliciclastic units in the Basque Basin (Ermua,
1123 Zumaia and Trabakua Pass), northern Spain. Palaeogeography, Palaeoclimatology, Palaeoeco-
1124 logy, 165, 299-320.
1125
1126 Schumm, S. A. (1985). Patterns of alluvial rivers. Annual Review of Earth and Planetary Sciences,
1127 13, 5-27.
1128
1129 Secord, R., Gingerich, P. D., Lohmann, K. C., & MacLeod, K. G. (2010). Continental warming pre-
1130 ceding the Palaeocene-Eocene thermal maximum. Nature, 467, 955-958.
1131
1132 Sinclair, H. D., Gibson, M., Naylor, M., & Morris, R. G. (2005). Asymmetric growth of the Pyrenees
1133 revealed through measurement and modeling of orogenic fluxes. American Journal of Science,
1134 305, 369-406.
1135
1136 Sluijs, A., Schouten, S., Pagani, M., Woltering, M., Brinkhuis, H., Sinninghe Damsté, J. S., Dick-
1137 ens, G. R., Huber, M., Reichart, G.-J., Stein, R., Matthiessen, J., Lourens, L.J., Pedentchouk, N.,
1138 Backman., J., Moran, K., & the Expedition 302 Scientists (2006). Subtropical Arctic Ocean temper-
1139 atures during the Palaeocene/Eocene thermal maximum. Nature, 441, 610-613.

1140

1141 Sluijs, A., Brinkhuis, H., Crouch, E. M., John, C. M., Handley, L., Munsterman, D., Bohaty, S.,
1142 Zachos, J. C., Reichart, G.-J., Schouten, S., Pancost, R. D., Sinninghe Damsté, J. S., Welters, N.
1143 L. D., Lotter, A. F., & Dickens, G. R. (2008). Eustatic variations during the Paleocene-Eocene
1144 greenhouse world. Paleoceanography, 23, PA4216.

1145

1146 Teixel, A., and Muñoz, J. A. (2000) Evolución tectono-sedimentaria del Pirineo meridional durante
1147 el Terciario: una síntesis basada en la transversal del río Noguera-Ribagorzana. Revista de la
1148 Sociedad Geológica de España, 13, 251-264.

1149

1150 Thorne, C. R. (1991). Bank erosion and meander migration of the Red and Mississippi Rivers,
1151 USA. In: Van-de-Ven, F. H. M., Gutknecht, D., Loucks, D. P., & Salewicz, K. A. (eds.) Hydrology for
1152 the water management of large river basins: Proceedings of the 20th General Assembly of the In-
1153 ternational Union of Geodesy and Geophysics. International Association of Hydrological Sciences
1154 Publication, 201, 301-313.

1155

1156 Tripati, A., & Elderfield, H. (2005). Deep-sea temperature and circulation changes at the Paleo-
1157 cene-Eocene Thermal Maximum. Science, 308, 1894-1898.

1158

1159 Vergés, J., & Burbank, D. W. (1996). Eocene-Oligocene thrusting and basin configuration in the
1160 eastern and central Pyrenees (Spain). In: Friend, P. F., & Dabrio C. R. (eds.), Tertiary Basins of
1161 Spain: The Stratigraphic Record of Crustal Kinematics, Cambridge University Press, Cambridge,
1162 120-133.

1163

1164 Vergés, J., Millán, H., Roca, E., Muñoz, J. A., Marzo, M., Cirés, J., den Bezemer, T., Zoetemeijer,
1165 R., & Cloetingh, S. (1995). Eastern Pyrenees and related foreland basins: pre-, syn-and post-

Whitchurch, A. L., Carter, A., Sinclair, H. D., Duller, R. A., Whittaker, A. C., & Allen, P. A. (2011). Sediment routing system evolution within a diachronously uplifting orogen: Insights from detrital zircon thermochronological analyses from the South-Central Pyrenees. American Journal of Science, 311, 442-482.

Wickert, A. D., Martin, J. M., Tal, M., Kim, W., Sheets, B., & Paola, C. (2013). River channel lateral mobility: metrics, time scales, and controls. Journal of Geophysical Research: Earth Surface, 118, 396-412.

Williams, G. D. (1985). Thrust tectonics in the south central Pyrenees. Journal of Structural Geology, 7, 11-17.

Williams, G. D., & Fischer, M. W. (1984). A balanced section across the Pyrenean orogenic belt. Tectonics, 3, 773-780.

Winguth, A., Shellito, C., Shields, C., & Winguth, C. (2010). Climate response at the Paleocene-Eocene thermal maximum to greenhouse gas forcing – A model study with CCSM3. Journal of Climate, 23, 2562-2584.

Wright, V. P., & Marriott, S. B. (1996). A quantitative approach to soil occurrence in alluvial deposits and its application to the Old Red Sandstone of Britain. Journal of the Geological Society, 153, 907-913.

Zachos, J. C., Wara, M. W., Bohaty, S., Delaney, M. L., Petrizzo, M. R., Brill, A., Bralower, T. J., & Premoli-Silva, I. (2003). A transient rise in tropical sea surface temperature during the Paleocene-Eocene thermal maximum. Science, 302, 1551-1554.

Zachos, J. C., Schouten, S., Bohaty, S., Quattlebaum, T., Sluijs, A., Brinkhuis, H., Gibbs, S.J., & Bralower, T. J. (2006). Extreme warming of mid-latitude coastal ocean during the Paleocene-Eocene Thermal Maximum: Inferences from TEX86 and isotope data. Geology, 34, 737-740.